Understanding the eco-geomorphologic feedback of coastal marsh under sea level rise: vegetation dynamic representations, processes interaction, and parametric sensitivity

Yu Zhang[1], Joel Rowland[1], Chonggang Xu[1], Phillip J. Wolfram[2], Daniil Svyatsky[2], J. David Moulton[2], Zhendong Cao[2], Marco Marani[3,4,5], Andrea D'Alpaos[6], and Donatella Pasqualini[7]

[1]Earth and Environmental Sciences Division, Los Alamos National Laboratory, Los Alamos, NM, USA.

[2]Theoretical Division, Los Alamos National Laboratory, Los Alamos, NM, USA.

[3]Division of Earth and Ocean Sciences, Duke University, Durham, NC, USA.

[4]Department of Civil and Environmental Engineering, Duke University, Durham, NC, USA.

[5]Dipartimento di Ingegneria Civile, Edile ed Ambientale, Universita' degli studi di Padova, Padova, Italy.

[6]Department of Geosciences, University of Padova, Via Gradenigo 6, 35131 Padova, Italy

[7]Analytics, Intelligence & Technology Division, Los Alamos National Laboratory, Los Alamos, NM, USA.

Corresponding author: Yu Zhang (yuzhang@lanl.gov)

Key Points:

- Spatial variations in marsh accretion rates must be evaluated to assess marsh resilience to sea level rise
- The evolution of simulated marsh elevations, biomass profiles, and parametric sensitivities depend on how vegetation is modelled
- Model parametric sensitivity varies with rates of future sea level rise

Abstract

A growing number of coastal eco-geomorphologic modeling studies have been conducted to understand coastal marsh evolution under sea level rise (SLR). Although these models quantify marsh topographic change as a function of sedimentation and erosion, their representations of vegetation dynamics that control organic sedimentation differ. How vegetation dynamic schemes and parameter values contribute to simulation outcomes is still not quantified. Additionally, the sensitivity of modeling outcomes on parameter selection in the available formulations has not been rigorously tested to date, especially under the influence of an accelerating SLR. This knowledge gap severely limits modeling accuracy and the estimation of the vulnerability of coastal marshes under SLR. In this paper, we used coastal eco-geomorphologic models with different vegetation dynamic schemes to investigate the eco-geomorphologic feedbacks of coastal marshes and parametric sensitivity under SLR scenarios. We found that marsh accretion rate near the seaward boundary can keep pace with moderate and high rates of SLR, while interior marsh regions are vulnerable to a high rate of SLR. The simulations with different vegetation schemes exhibit diversity in elevation and biomass profiles and parametric sensitivity. We also found that the model parametric sensitivity varies with rates of future SLR. Vegetation-related parameters and sediment diffusivity, which are not well measured or discussed in previous studies, are identified as some of the most critical parameters. Our findings provide insights to appropriately choose modeling presentations of key processes and feedbacks for different coastal marsh landscapes under SLR, which has practical implications for coastal ecosystem management and protection.

Keywords: Landscape evolution, Eco-geomorphologic model, Coastal marsh, Sea level rise, Accretion, Vulnerability

1 Introduction

Coastal marshes are unique landscapes that connect terrestrial and aquatic systems and provide important ecosystem services, such as sustaining wildlife habitats, protecting shorelines, attenuating floods, storing carbon, and filtering contaminants (Barbier et al., 2011; Costanza et al., 1997; FitzGerald & Hughes, 2019; Roulet, 1990; Tiner, 2013). Intensified climate change, especially accelerating sea level rise (SLR), and reduced sediment transport to the coastal zone threaten the stability of coastal marsh ecosystems (Cahoon & Guntenspergen, 2010; Ratliff et al., 2015; Scavia et al., 2002; Yousefi Lalimi et al., 2020). The vertical accretion rate for coastal marsh surfaces is the difference between the sedimentation rate and the surface erosion rate and is controlled by complex eco-geomorphologic interactions at multiple scales. To survive, the vertical accretion rate must at least keep pace with the rate of relative SLR (i.e. SLR + subsidence rate, Burkett & Kusler, 2000; Day et al., 2008; Kirwan et al., 2010; Marani et al., 2007; Reed, 1995). Therefore, investigating how eco-geomorphologic processes respond to SLR is a prerequisite for understanding the sustainability and resilience of coastal ecosystem structure and functions to SLR.

The term eco-geomorphology, which highlights the interactions between landscapes and ecosystems, can be traced back to the concept of bio-geomorphology in the pioneering study by *Viles* [1988], who explicitly considered the interactive roles of biota and geomorphology in landscape development. Later, a more comprehensive description of the linkage between coastal hydrology, vegetation dynamics, and geomorphology was gradually established by early-stage modeling studies (Allen, 2000; D'Alpaos et al., 2007; French, 1993; Kirwan & Murray, 2007; Marani et al., 2007; Morris et al., 2002; Mudd et al., 2004, 2009; Randerson, 1979; van Wijnen & Bakker, 2001). The diagram presented in Figure 1 includes the key components that control

the eco-geomorphologic feedbacks in coastal ecosystems and provides a conceptual framework for model development and analysis. Here, the state and dynamics of a hydro-eco-geomorphic system is described in terms of three variables (marsh elevation, vegetation biomass, and ocean drivers including saltwater intrusion, tide, wave, storm surge, and sea level rise (SLR)) and three sediment fluxes (inorganic sediment deposition, organic soil production, and erosion) (Allen, 2000; Marani et al., 2007, 2010). The elevation of marshland with respect to the mean sea level, which may change over time, is controlled by accretion through inorganic sediment deposition, organic soil production, and erosion, as well as by land subsidence (soil compaction and sediment decomposition) and SLR. Tidal currents, waves, and storm surges directly drive sediment dynamics via sediment deposition and erosion. Changes in tidal currents affect the frequency and duration of flooding of marsh plants, and therefore changes soil salinity, oxygen and sulfide availability affecting plant growth (Silvestri & Marani, 2004). Vegetation plays a critical role in decreasing water velocity and dissipating wave energy, thereby reducing sediment erosion and increasing deposition (Carus et al., 2016; Ghisalberti & Nepf, 2005; Moller et al., 2014; Nepf, 1999; Yang et al., 2012). Vegetation also contributes to sedimentation by directly trapping suspended sediment and by producing organic matters in soil (Mudd et al., 2004). Changes in marsh elevation produce changes in water levels on marshland, thereby affecting marsh plant development (Morris et al., 2002; Mudd et al., 2004).

Using this conceptual framework, a number of mathematical models have been developed to describe and understand the evolution of coastal marshes under SLR (e.g., Allen, 2000; Best et al., 2018; Da Lio et al., 2013; D'Alpaos et al., 2007; Duvall et al., 2019; French, 1993, 2006; Kirwan et al., 2010; Kirwan, Temmerman, et al., 2016; Kirwan, Walters, et al., 2016; Kirwan & Murray, 2007; Kirwan & Temmerman, 2009; Marani et al., 2007, 2013;

Mariotti & Fagherazzi, 2010; Morris & Bowden, 1986; Mudd et al., 2009; Rogers et al., 2012; Schile et al., 2014; Schuerch et al., 2018; Stralberg et al., 2011; van Wijnen & Bakker, 2001). Although these models vary in complexity, all provide insights into coastal marsh vulnerability under SLR, especially for understanding whether the accretion rate of marshland can keep pace with the rate of SLR.

In terms of their representation of vegetation-related processes, some studies assumed static vegetation with a constant influence of vegetation on hydrodynamics and sedimentation (Allen, 1995; D'Alpaos et al., 2011; French, 1993; Mudd et al., 2009; Rogers et al., 2012; Schile et al., 2014; Stralberg et al., 2011; van Wijnen & Bakker, 2001). Other studies modeled more detailed vegetation-water-land interactions by considering vegetation density, height, and submergence condition and how they impact water flow and sediment transport (e.g., Da Lio et al., 2013; D'Alpaos et al., 2007; Duvall et al., 2019; Mudd et al., 2004, 2009; Temmerman et al., 2005). *Morris et al.* (2002) first proposed a clear relationship between marsh vegetation biomass and its depth below mean highest tide level based on the field observation on the coastal marsh in South Carolina, USA. Other studies extended this work to explicitly integrate quantitative representations for vegetation dynamics into coastal marsh evolution by assuming 1) a linear relationship between *Spartina*-dominant vegetation and its ponding condition (Belliard et al., 2015; D'Alpaos et al., 2007), 2) a nonlinear relationship between *Spartina*-dominant vegetation and its ponding condition (Kirwan & Murray, 2007; Mariotti & Fagherazzi, 2010), or 3) a linear relationship between multiple vegetation species and their ponding condition (Belliard et al., 2015; D'Alpaos et al., 2007, 2019; Marani et al., 2004, 2013; Silvestri et al., 2005). The detailed explanations are presented in Subsection 2.1.

Many of these modeling studies evaluated the vulnerability of coastal marshes under SLR by using a lumped approach, where they treated coastal marshes as a single point or only focused on the marsh near the seaward boundary without an examination of the marsh spatial variation from the ocean to the upland in responding to SLR (D'Alpaos et al., 2011; French, 2006; Kirwan et al., 2010; Kirwan & Temmerman, 2009; Mudd et al., 2009; Temmerman et al., 2003; van Wijnen & Bakker, 2001). Other studies investigated the spatial and temporal variation of coastal marsh evolution under SLR (D'Alpaos et al., 2007; D'Alpaos & Marani, 2016; Kirwan, Walters, et al., 2016; Marani et al., 2013; Ratliff et al., 2015). However, the response of coastal marsh evolution under SLR to varying representations of vegetation dynamic processes is still not well understood, especially in terms of the co-evolution of coastal marsh elevation and vegetation. Furthermore, as the complexity and sophistication of these coastal models continues to increase, there is a critical knowledge gap in how sensitive model predictions are to model parameterizations under different SLR conditions. This knowledge is critical for developing effective model parameterizations, and designing field studies to constrain those model parameters under different SLR scenarios. Currently, this knowledge gap limits our confidence in the application of these types of models to inform coastal wetland management and protection.

In this study, we use two coastal eco-geomorphic models with different vegetation dynamic representations to investigate the eco-geomorphologic feedbacks in coastal marshes under future SLR conditions to address the following two questions:

1) How will the selection of vegetation representations result in spatial and temporal variations in eco-geomorphologic outcomes of coastal marshes under SLR?
2) How will the different vegetation representations and different rates of SLR affect model parametric sensitivity?

142 To address these questions we simulate the evolution of a one-dimensional coastal marsh
143 transect using two well-established coastal eco-geomorphologic models from *D'Alpaos et al.*
144 (2007) and *Mariotti and Fagherazzi* (2010). Specifically, under two commonly-used future
145 global mean SLR scenarios (SLR=0.01 m/yr and SLR=0.005 m/yr, corresponding to RCP 4.5
146 and RCP 8.5 scenarios in Phase 5 of the Coupled Model Intercomparison Project (CMIP5)
147 (Spencer et al., 2016), we explored three different dependencies of vegetation biomass on
148 elevation above mean sea-level: linear and non-linear formulations for the *Spartina*-dominant
149 vegetation (D'Alpaos et al., 2007; Mariotti & Fagherazzi, 2010; Morris et al., 2002); and the
150 mixed-species linear function (D'Alpaos et al., 2007). After comparing the spatial and temporal
151 variations of coastal marsh evolution under SLR with different vegetation equations, we used a
152 global sensitivity approach to evaluate the sensitivity of eco-geomorphologic processes to model
153 parameterizations spanning a wide range of the parameters.

154 The paper begins by introducing process representation in Section 2, followed by model
155 introduction, study site, experiment design, and model setting in Section 3. Then we analyze the
156 marsh evolution and model sensitivity under different rates of sea level rise, vegetation schemes,
157 and maximum organic soil production rates in Section 4. Finally, we discuss the implications of
158 this study for understanding the vulnerability of coastal marsh under SLR, guiding data-model
159 integration, representation, and uncertainties. These results should provide valuable insights to
160 appropriately choose process representations in modeling and identify key parameters for
161 different coastal marsh landscapes under SLR.

162 **2. Background: process representation in eco-geomorphologic models**

163 In general, the current generation of eco-geomorphologic models represents topographic
164 change of coastal marsh as the net balance of sediment erosion and deposition (Fagherazzi et al.,

2012). Based on mass conservation, the spatially-averaged dynamics of topographic elevation in a coastal landscape can be expressed as

$$\frac{dz}{dt} = \frac{1}{1-p}(D - E) - R, \quad (1)$$

where z is the surface elevation relative to the mean sea level with the dimension of [L]; t is time [T]; p is the porosity of bed sediment; D and E represent local sediment deposition and erosion rates with the dimensions of [L/T], respectively; and R is the rate of sea level rise [L/T].

However, the way each term in Eq. 1 is modeled may vary. For the erosion term (E) in Eq. 1, it may consist of erosion due to bed shear stress induced by currents and waves and/or due to wave breaking (Carniello et al., 2005; Marani et al., 2010; Mariotti & Fagherazzi, 2010; Van Rijn, 1993), namely,

$$E = E_{shear} + E_{break}, \quad (2)$$

where E_{shear} is the erosion due to bed shear stress. Erosion occurs when the bed shear stress (τ_0) exceeds the critical shear stress for erosion (τ_e), viz

$$E_{shear} = \begin{cases} \alpha\left(\frac{\tau_0}{\tau_e} - 1\right) & if\ \tau_0 > \tau_e \\ 0 & if\ \tau_0 < \tau_e \end{cases}, \quad (3)$$

where α is the erosion coefficient. E_{break} in Eq. 2 is the erosion due to wave breaking. According to *Mariotti and Fagherazzi* (2010), E_{break} is a function of wave power dissipated by breaking:

$$E_{break} = \begin{cases} \beta\left(\frac{P}{P_{cr}} - 1\right)/d & if\ P > P_{cr} \\ 0 & if\ P < P_{cr} \end{cases}, \quad (4)$$

where β is the wave erosion coefficient; P is the wave power per unit area; P_{cr} is the threshold of wave power for wave erosion; and d is the spatial interval over which wave breaking occurs.

The sedimentation rate, D in Eq. 1, is given by

$$D = D_s + D_t + D_o, \tag{5}$$

where D_s is the inorganic sediment settling rate [L/T], which is a function of settling velocity (w_s) (Cao et al., 2020), suspended sediment concentration (C), bed shear stress (τ_0) due to water flow, and critical shear stress for sedimentation (τ_d) (Krone, 1962), namely,

$$D_s = \begin{cases} w_s C\left(1 - \frac{\tau_0}{\tau_d}\right) & if\ \tau_0 < \tau_d \\ 0 & if\ \tau_0 > \tau_d \end{cases}. \tag{6}$$

D_t in Eq. 5 is the inorganic sediment trapping rate due to the effect of vegetation canopy [L/T], which can be represented by an empirical form

$$D_t = CU\epsilon d_s n_s \min[h_s, h_w] \tag{7}$$

where U is the water flow velocity [L/T]; ϵ is a capture efficiency of vegetation stems, h_w is the water flow depth [L], and several vegetation characteristics, such as plant stem diameter (d_s), stem density (n_s), and vegetation height (h_s) (Mudd et al., 2004; Palmer et al., 2004). Additionally, D_o in Eq. 5 is the organic matter production rate [L/T], which is a function of plant biomass, viz

$$D_o = K_b \frac{B}{B_{max}}, \tag{8}$$

where K_b is the maximum production rate of below ground organic material; B is the biomass at the current time; and B_{max} is the maximum vegetation biomass. The growth of coastal marsh vegetation is controlled by several factors related to nutrient inputs (e.g., nitrogen and

phosphorous) and soil environmental stress (e.g., oxygen availability, salinity, and sulfide concentration) (Silvestri & Marani, 2004) *Morris et al.* (2002) proposed a relation between vegetation biomass and the depth of the marsh surface below the mean highest tidal level based on observations at a coastal marsh in South Carolina. Based on this relation, several empirical functions were derived to represent equilibrium vegetation biomass under different ponding conditions. The empirical function can be expressed as a linear (D'Alpaos et al., 2007) or a parabolic (Morris et al., 2002) function of salt marsh elevation relative to tide level. For the linear dependency, current modeling studies also considered the different response of marsh species to sea level change (see Fig. 2). For example, the lowland area with frequent flooding is more favorable for salt-tolerant and flood-tolerant species, such as *Spartina alterniflora*. Quantitatively, the biomass equation can be written as (see the blue line in Fig. 2)

$$B_1 = \begin{cases} \left(\frac{MHTL - D_{biomin} - z)}{D_{biomax} - D_{biomin}}\right) B_{max} & if\ MHTL - D_{biomax} \le z \le MHTL - D_{biomin} \\ 0 & if\ MHTL - D_{biomax} > z\ or\ z > MHTL - D_{biomin} \end{cases}, \quad (9)$$

where B_1 is the time-averaged belowground biomass density [M/L^2]; B_{max} is the maximum biomass density [M/L^2]; $MHTL$ represents the mean highest tide level [L]; D_{biomax} and D_{biomin} are the highest and lowest depth below *MHTL*, respectively, which bounds the upper and lower limits of vegetation growth range (D'Alpaos et al., 2007). $MHTL - D_{biomin}$ and $MHTL - D_{biomax}$ represent the elevations of the upper and lower boundaries for vegetation growth (the dashed lines in Fig. 2). Whereas, some mixed species on marshland prefer higher elevation region with less flooding and better aerated soil (see the orange line in Fig. 2), namely

$$B_2 = \begin{cases} 0 & if\ MHTL - D_{biomax} > z \\ \left(\frac{z - (MHTL - D_{biomax})}{D_{biomax} - D_{biomin}}\right) B_{max} & if\ MHTL - D_{biomax} \le z \le MHTL - D_{biomin} \\ B_{max} & if\ z > MHTL - D_{biomin} \end{cases}, \quad (10)$$

where B_2 is the time-averaged belowground biomass density for mixed species [M/L^2] (D'Alpaos et al., 2007). Besides these linear functions, a parabolic formulation describes that the plant biomass goes to zero when the marsh surface elevation reaches the upper ($MHTL - D_{biomin}$) or lower bound ($MHTL - D_{biomax}$), and the biomass reaches its peak at a certain elevation between $MHTL - D_{biomin}$ and $MHTL - D_{biomax}$ (see the yellow line in Fig. 2):

$$B_3 = \begin{cases} 0 & if\ MHTL - D_{biomax} > z\ or\ z > MHTL - D_{biomin} \\ B_{max}(aD + bD^2 + c) & if\ MHTL - D_{biomax} \le z \le MHTL - D_{biomin} \end{cases}, \quad (11)$$

where B_3 is the time-averaged belowground biomass density [M/L^2] (Morris, 2006); D is the ratio between $MHTL - D_{biomin} - z$ and $D_{biomax} - D_{biomin}$; *a*, *b*, and *c* are fitting coefficients.

The representation of marsh hydrodynamics driven by tides and waves is also an essential part of eco-geomorphologic modeling because both erosion and sedimentation are fundamentally tied to surface water flow (Scheidegger, 1961). The shallow water equations, derived from the depth-integrated Navier–Stokes equations, have been widely used to compute hydrodynamics in coastal regions where the water horizontal length scale is much greater than the vertical length scale (Vreugdenhil, 2013). Specifically, the shallow water equations consist of two conservation equations: 1) conservation of mass and 2) conservation of momentum. Namely, in a one-dimensional (1-D) domain,

$$Conservation\ of\ mass: \frac{\partial \eta}{\partial t} + \frac{\partial (\eta u)}{\partial x} = 0, \quad (12)$$

and

$$Conservation\ of\ momentum: \frac{\partial u}{\partial t} + u\frac{\partial (u)}{\partial x} = -g\frac{\partial (h)}{\partial x} - g\frac{u|u|}{C^2 h} = 0, \quad (13)$$

where h is the water surface elevation = land surface elevation (z) + local water flow depth (η) [L], thus h varies not only depending on the change in water depth, but also the simultaneous morphological change; u is the flow velocity [L/T]; g is the gravitational acceleration [L/T^2]; x is the spatial direction along the 1-D domain [L]; and C is the Chezy's friction coefficient.

3 Methodology

3.1 Numerical model

We used a 1-D version of the coastal eco-geomorphologic model developed by *D'Alpaos et al.* (2007) (hereinafter referred to as D-model) focusing on the interaction between land and ocean without lateral water and sediment fluxes, such as tidal channels. The D-model integrates all the hydro-eco-geomorphologic components introduced in Fig. 1, including sediment settling (Eq. 6), sediment trapping (Eq. 7), vegetation organic matter production (Eq. 8), and sediment erosion (Eq. 3), except sediment erosion due to waves which is of minimal importance for this problem. Because the effect of waves in controlling the spatial and temporal variation of coastal marsh evolution was well studied by *Duvall et al.* (2019) and *Mariotti and Fagherazzi* (2010), and vegetation can significantly mitigate waves if the waves are not too strong, wave-induced erosion is not a focus in this study. We focused on conditions with regular semi-diurnal tidal cycle and background SLR. For the representation of vegetation biomass, the original D-model included functions (e.g., Eqs. 9 and 10) that assume a linear relationship between annual averaged biomass and the elevation relative to mean sea level and considered different responses of *Spartina* and mixed vegetation species (see details in Subsection 2.1). To have a comprehensive understanding of the differences of the eco-geomorphologic feedbacks under different representations of vegetation dynamics, we integrated the nonlinear function

(e.g., Eq. 11) into the D-model as well. For the computation of hydrodynamics, the D-model uses an approach similar to the kinematic-wave form that assumes a balance between water surface slope and friction in the momentum equation (Eq. 13) (D'Alpaos et al., 2007; Rinaldo et al., 1999). The detail of the hydrodynamic component is referred to the supplementary information S1 and *D'Alpaos et al.* (2007), and the detail for the sediment transport component is referred to Section 2 above and *D'Alpaos et al.* (2007).

To demonstrate that the D-model appropriately captures the behavior of coastal evolution under SLR, we conducted some of the same simulations by using another well-established coastal eco-geomorphologic model developed by *Mariotti and Fagherrazi* (2010) (hereinafter referred to as M-model). Similar to the D-model, the M-model integrates all the hydro-eco-geomorphological components introduced in Fig. 1, including sediment settling (Eq. 6), sediment trapping (Eq. 7), vegetation organic matter production (Eq. 8), and sediment erosion (Eq. 3), as well as sediment erosion due to waves (Eq. 4). To make the simulations from the D- and M-model comparable, we turned off the process of erosion due to waves in the M-model. For the representation of vegetation biomass, the M-model uses the Spartina-dominant nonlinear function, the same function we added to the D-model. An introduction to the M-model and its simulation results may be found in the supplementary information S2 and in *Mariotti and Fagherazzi* (2010).

3.2 Numerical Experiment

We used a 1-D transect based on a marsh platform along the Delaware Bay, USA, as a prototype for our simulations (the black solid line in Fig. 3c). Marsh surface elevation in the 1-D transect is at a level close to MHTL (gray dashed line in Fig. 3c), consistent with observations in Delaware Bay based on the CoNED coastal elevation database (Danielson et al.,

2016) and NOAA (National Oceanic and Atmospheric Administration) tide observations (NOAA, 2001), which indicates that the landscape is at or close to an equilibrium state under the current sea level conditions (D'Alpaos et al., 2007).

This study simplifies the 1-D transect topography by using a linear interpolation of the observed topography (red line in Fig. 3c) as the initial land surface elevation for the numerical experiments. The origin of the 1-D model domain is placed at the seaward boundary (x=0), whereas the upland boundary is located at x=L. Water and sediment can only flow through the seaward boundary with zero flux flowing through the upland boundary. The current mean sea level (MSL) is at -0.13 m above NAVD88 (North American Vertical Datum of 1988), and the averaged tide amplitude is about 0.8 m based on the NOAA tide and current observation at station Cape May, NJ [8536110] (the red star in Fig. 3b). We used a constant suspended sediment concentration (C_0=20 mg/L) at the ocean boundary (x=0). The value of C_0 falls at the lower bound of the range of sediment concentration used in the previous coastal eco-geomorphologic modeling studies (e.g., Kirwan, Walters, et al., 2016). Thus, this study makes a conservative prediction of coastal marsh change under SLR. However, a comparable numerical experiment with the same model settings but with a higher suspended sediment concentration (C_0=100 mg/L) was also conducted, and the results can be found in the supplementary information.

In order to speed-up simulations to geomorphologically relevant time scales, the simulations adopted a morphological scaling factor (MSF, e.g., *Lesser et al.* (2004); Roelvink (2006); Zhang et al (2016)), which effectively assumes that changes in the topographic profile over time scales smaller than the scaling factor do not appreciably affect the flow field and the eco-geomorphic dynamics. Hence, elevation change is computed offline by applying sediment

311 fluxes determined in a tidal cycle, assumed to be constant for a period of time equal to the MSF.
312 Thus, in this study, the simulations were run for 500 years (consistent with the simulation time
313 in *D'Alpaos et al.* (2007) to make sure the landscape reaches an equilibrium state) with a spatial
314 interval of 1 m and a time interval of 10 minutes for hydrodynamics and MSF=50 for the eco-
315 geomorphologic change. The same numerical settings were applied to the M-model simulations
316 in the supplementary information.

317 We designed several focused numerical experiments to characterize eco-
318 geomorphologic feedbacks under different representations of vegetation dynamics and SLR
319 scenarios for the future 500 years. We adopted two commonly used future global mean SLR
320 scenarios from global climate model predictions, including (1) the relatively low SLR rate
321 (0.005 m/yr) (Da Lio et al., 2013; Ganju et al., 2020; Kirwan & Temmerman, 2009; Spencer et
322 al., 2016) and (2) the relatively high rate of SLR (0.01 m/yr) (Ganju et al., 2020; Kirwan,
323 Walters, et al., 2016; Orson et al., 1985; Spencer et al., 2016). In addition, we considered three
324 different representations of vegetation dynamic processes, such as the Spartina-dominant linear
325 function, Spartina-dominant nonlinear function, and mixed species linear function. Also, in
326 simulating vegetation organic soil production, we incorporated two different rates of maximum
327 organic production rates: 1) $K_b = 0.003\ m/yr$, a commonly used maximum organic production
328 rate under current climate (Mudd et al., 2009) and 2) $K_b = 0.009\ m/yr$, a larger maximum
329 organic production rate used in the previous modeling studies (e.g., Mariotti & Fagherazzi,
330 2010), reflecting the increase of belowground biomass productivity under elevated atmospheric
331 CO_2 in the future (Ratliff et al., 2015). Scenario details are listed in Table 1. The parameters for
332 these individual simulations are listed in the fourth column in Table 2.

3.3 Sensitivity analysis

There are many sensitivity analysis approaches available to understand parametric sensitivity of model behavior (see *Song et al*. (2015) for a detailed review). In this study, we used a widely applied sensitivity analysis approach, the Fourier Amplitude Sensitivity Test (FAST) technique (Cukier et al., 1973; Xu & Gertner, 2011, 2008a). FAST is computationally efficient and can be used for both nonlinear and non-monotonic relationships between parameters and model outputs (Xu & Gertner, 2011). FAST uses a periodic sampling strategy to assign a characteristic periodic signal for each parameter. Within FAST, a Fourier transformation is used to decompose the variance in model outputs into partial variance contributions by individual model parameters based on the assigned signals. The ratio of partial variance contributed by a specific parameter to the total variance of a model output is defined as the first-order sensitivity index to measure the importance of each model parameter. The FAST analysis has been incorporated into a software tool, the UASA ToolBox (https://sites.google.com/site/xuchongang/uasatoolbox) by *Xu and Gertner (2008b)* and provides a rigorous way of defining, executing, and analyzing experiments for model parametric sensitivity.

This study selected 11 common parameters that have been used in many coastal eco-geomorphologic models including the D and M models (see the list of the parameters in Table. 2). Based on this selection, the UASA ToolBox was used to generate 1,100 groups of parameters for the model ensemble simulations to quantify the models' individual parametric sensitivities. The range of each parameter is estimated based on our literature survey and empirical knowledge. However, because there is not enough data to derive informative probability density distributions, we used a uniform distribution for our sensitivity analysis.

Model sensitivity is defined in terms of relevant quantitative metrics describing the final state of the system: 1) the difference between the MHTL and the elevation at the seaward boundary (MHTL minus elevation, hereinafter referred to as *Depth_m*), 2) the difference between the elevations at the seaward and upland boundaries (elevation relief) from each ensemble simulation under different scenarios, 3) domain averaged sediment fluxes, 4) the vegetation biomass at the seaward boundary, and 5) the vegetation biomass at the upland boundary. Notably, the first metric, Depth_m, measures how the landscape elevation (at least the seaward boundary) responds to SLR. While the second metric (elevation relief) measures the difference of elevation at the seaward boundary and inland and possible inland depression on the 1-D profile.

4. Results

4.1 Topographic evolution and sediment fluxes under different SLR rates

4.1.1 Topographic change across individual simulations

We first used twelve individual simulations (cases 1 to 12 in Table. 1) as examples to compare the elevation change under different vegetation equations for biomass estimation and SLR scenarios simulated by the D-model over 500 years (see Fig. 4). The corresponding sediment fluxes at the end of the 500 years are illustrated in Fig. 5. Domain-wide, the elevations in the cases with a higher maximum organic production rate (K_b) (the first column in Fig. 4) were higher than the elevation in the lower K_b cases (the second column in Fig. 4). At the seaward boundary, the relative locations between elevation and MHTL near the seaward boundary in all vegetation-covered scenarios remained constant after 400 years' simulation (not shown at here) due to a balance between sediment fluxes (Fig. 5), which indicate that 1) the

elevations near the seaward boundary reached a new equilibrium state under future SLR and 2) the marshland near the seaward boundary kept pace with the rates of SLR. In contrast, the cases without vegetation showed clear declines of elevation near the ocean boundary (gray dashed lines in Fig. 4) due to erosion (the black lines in Fig. 5d and k) and lack of organic accretion and inorganic trapping. The final elevations with vegetation coverage reached the level of MHTL (solid lines in Fig. 4), except in the high SLR and low K_b scenario (Fig. 4c), where the elevation was 0.2-0.3 m below the MHTL, and in the low SLR and high K_b scenario (Fig. 4b), where the simulated marsh surface elevation with the mixed-vegetation equation (hereinafter referred to as mixed-veg case) was higher than the MHTL.

Moving landward, the marsh elevations declined due to a decrease in sedimentation rate landward. Some of the marshland became totally submerged in water as the elevation was below the final mean sea level (final MSL indicated by the blue dashed lines in Fig. 4). With a higher K_b, a shorter portion of the marshland was below the final MSL because a higher K_b resulted in a higher organic sedimentation rate, which dominantly contributed to the accretion rate at the upland area where inorganic sediment from the ocean was restricted to this region.

High SLR caused a larger elevation relief ranging from a maximum of 3.5 m under the higher K_b case (Fig. 4a) to 5m under the lower K_b case (Fig. 4c), compared to the low SLR scenarios that only had a maximum elevation relief of 0.48 m in the higher K_b case (Fig. 4b) and 2.85m in the lower K_b case (Fig. 4d), respectively. Notably, in the lower SLR scenario with a higher K_b, the elevation slightly declined landward (Solid lines in Fig. 4b), which means that the net sedimentation rate always kept pace with the rate of SLR as illustrated in Fig. 5h, i, and j.

Different vegetation schemes also highlight different influences on the topographic outcomes. Among all the vegetation cases, the Spartina-nonlinear case showed the highest final elevation and the least elevation relief due to the highest sedimentation rate throughout the domain, particularly due to organic soil production in the middle and upper portions of the transect. In terms of the elevation decline, the decline started earlier in the mixed-veg cases (at approximately 100 to 200 m from the seaward boundary) than the elevations with Spartina-dominant linear and nonlinear functions (hereinafter referred to as Spartina-linear case and Spartina-nonlinear case, respectively) which started to decline around 250 to 350 m away from the seaward boundary (thick and thin black solid lines in Fig. 4). Notably, in the mixed-veg case under low SLR and high K_b (gray solid line in Fig. 4b), the elevation rose above MHTL and ended at 1 meter above MHTL. This was because the vegetation growth in the mixed-veg case is greater at lower inundation levels. Thus, vegetation continued growing even when the elevation is above the MHTL. The 1-meter height is constrained by the assumption of 1-meter root depth in the model simulation. If the land surface exceeds 1 m, the vegetation biomass decreases rapidly because the model assumes that vegetation cannot access enough water in the soil and the halophytic vegetation species would be out competed by other terrestrial species. In the Spartina-dominant cases, the Spartina-nonlinear cases showed a starting of elevation decline closer to the seaward boundary than the elevation decline in the Spartina-linear cases (black solid lines in Fig 4a, c, and d).

For the contributions of sediment fluxes to marshland accretion, in general, sediment settling rate contributed more than sediment trapping rate and organic production rate near the seaward boundary (light blue lines in Fig. 5) in all vegetation-covered cases, except the mixed-veg cases (Fig. 5c, j, and n) where the organic production rate was higher than the other fluxes.

423 This is because the mixed-veg case assumes that vegetation can grow better under lower
424 inundation or no inundation conditions where vegetation organic production always plays a role
425 in contributing to marsh accretion, but inorganic sediment settling contributes less due to
426 limited delivery of sediment to marshland. Given that the elevation near the seaward boundary
427 accreted faster than the inland area, the inundation depth near the seaward boundary was
428 shallower than the inland, which provided a more favorable condition for mixed vegetation
429 species to grow near the seaward boundary, resulting in a higher organic production rate there.

430 Moving landward, the contributions of fluxes to the accretion rate varied spatially across
431 different K_b cases, SLR conditions, and vegetation schemes (Fig. 5). Under higher K_b, the
432 organic production rate was dominant (purple lines in Fig. 5a, b, c, h, i, and j), and the spatial
433 patterns of the sediment fluxes reflected the different assumptions of the vegetation schemes.
434 For example, the patterns of fluxes were very different between the mixed-veg case and
435 Spartina-dominant case due to the different assumptions of the favorable growth condition for
436 vegetation. In contrast, in the lower K_b cases, the low vegetation organic production rate limited
437 the vegetation effect in controlling accretion rate. Thus, the sediment settling rate was dominant
438 landward in the lower K_b cases. We also observed that the vegetation-related fluxes (sediment
439 trapping and organic production) were overall higher in the high SLR scenarios than in their
440 corresponding low SLR scenarios. We did not observe erosion under this regular tidal cycle
441 and sea level rise condition in the vegetation-covered cases because vegetation reduced water
442 flow velocity and prevented erosion in these experiments.

443 **4.1.2 Model parametric sensitivity from ensemble simulations**

444 We explored the model parametric sensitivity represented by the ratio of individual
445 parametric variance to the total variance from the ensemble simulations across different

combination of parameters spanning wide ranges of their values (see Table. 2). This analysis captured the overall parametric sensitivity of the eco-geomorphologic processes in the model and highlighted how different representations of vegetation dynamics and SLR conditions affect the parametric sensitivity.

4.1.2.1 Parametric sensitivity for topographic change

For the sensitivity of modeled *Depth_m* (defined as MHTL minus elevation in Subsection 3.3) to parameterization (Fig. 6a), vegetation-related parameters showed a larger influence on *Depth_m* under the higher rate of SLR (e.g., the first three columns in Fig.6a). While, under the lower rate of SLR, the sediment-related parameters, especially the "sediment concentration", were the dominant parameters (the last three columns in Fig. 6a). For the different vegetation dynamic schemes, the mixed-veg cases were highly sensitive to the "maximum organic production rate" indicating that the elevation at the seaward boundary relative to the MHTL was highly dependent on the organic matter production rate regardless of the rates of SLR because some species in the mixed-veg cases can grow under more prolonged flooding condition, and the other species are adapted to less frequent and prolonged flooding condition, such that the vegetation processes can contribute to sedimentation in all conditions. While, in the *Spartina*-dominant cases, the vegetation can only grow under more prolonged flooding condition driven by SLR and tide. Thus, the parametric sensitivities in the *Spartina* linear and nonlinear cases (the first, second, fourth, and fifth columns in Fig. 6a) were controlled by the inundation condition, the sediment settling, and vegetation processes and did not present a huge difference among parameters, compared to the mixed-veg cases. The relatively more sensitive parameters are "maximum organic production rate", "maximum biomass", "water depth for plant growth", "sed concentration", and "critical shear stress for

deposition". Among these parameters, the "maximum organic production rate" was the most sensitive parameter in the high SLR scenario (the first and second columns inf Fig. 6a). In contrast, "sediment concentration" was the most sensitive parameter in the low SLR scenarios (the fourth and fifth columns in Fig. 6a). This is because the high rate of SLR has a larger potential to cause a higher inundation condition by high tides, a favorable condition for *Spartina* to grow. Therefore, the vegetation effect had a larger contribution to sedimentation than the contribution from vegetation in the low SLR cases.

For the sensitivity of elevation relief, in the high SLR scenario (the first, second, and third columns in Fig. 6b), the model simulations were more sensitive to the "sediment diffusivity" parameter, an important parameter in the sediment diffusion equation that controls how much sediment could propagate landward. "Tide amplitude" was also one of the most sensitive parameters in the Spartina-linear and -nonlinear cases. The vegetation-related parameters showed relatively low sensitivity (the first and second columns in Fig. 6b), which means that the elevation relief under high SLR was more dependent on how much sediment can propagate landward and deposit. However, in the mixed-veg case, the "maximum organic production rate" along with "sediment diffusivity" were the most sensitive parameters, which reflects the tolerance of the growth of mixed vegetation species in different conditions. For the low SLR scenario (the fourth to sixth columns), the vegetation-related parameters showed higher sensitivity, which means that the vegetation processes were more dominant to the change of elevation relief, especially for the Spartina-linear and nonlinear cases. The values of sensitivity for each parameter in each scenario can be found in Tables S1 and S2.

4.1.2.2 Parametric sensitivity for sediment fluxes

In terms of the parametric sensitivity of sediment fluxes to model parameterization, the sensitivities are similar to corresponding vegetation cases under both SLR scenarios. For example, the Spartina-linear cases (the first to third columns in Fig. 7a and first to third columns in Fig. 7b) under both the high and low SLR scenarios show a similar parametric sensitivity for each corresponding sedimentation processes.

Specifically, for the sediment settling process, all the cases (the first, fourth, and seventh columns in Fig. 7a and the first, fourth, and seventh columns in Fig. 7b) were most sensitive to the "maximum organic production rate", which may be because the organic production influences elevation changes that indirectly control sediment settling process. Besides the "maximum organic production rate", the model simulations were also sensitive to some sediment settling-related parameters, such as "sediment concentration", "settling velocity", and "critical shear stress for deposition", which are the key parameters directly control sediment settling process. For the organic soil production by vegetation, all the cases (the second, fifth, and eighth columns in Fig. 7a and the second, fifth, and eighth columns in Fig. 7b) were most sensitive to the "maximum organic production rate", the key parameter in organic soil production process. For the sediment trapping process, the sensitivity was almost evenly distributed for each parameter because sediment settling, sediment diffusion and advection, and vegetation all influence sediment trapping, however, the parameters of "sediment diffusivity" and "sediment concentration" that control the distribution of sediment concentration showed slightly higher sensitivity. The values of sensitivity for each parameter in each scenario can be found in Tables S3 and S4.

4.2 Vegetation dynamics with the change in surface topography

513 **4.2.1 The spatial and temporal variation of vegetation biomass from individual simulations**

514 The different formulations for vegetation growth in response to inundation conditions
515 (Fig. 2) lead to distinct patterns in biomass distributions and marsh response to tidal and SLR
516 induced flooding. Figure 8 showed the spatial variation of vegetation biomass at the end of 500
517 years in the simulations under the different vegetation dynamic schemes, rates of SLR, and K_bs.
518 In general, the spatial patterns of vegetation biomass corresponded to the marsh elevation
519 profiles in Fig. 4. For example, the locations of dramatic declines of vegetation biomass in the
520 high SLR scenarios are well-aligned with the topographical depression area in Fig. 4a and c. In
521 this low-lying region, the marsh elevations approach an unfavorable inundation condition for
522 vegetation growth with high ponding water detrimental to vegetation growth. In contrast, the
523 spatial variations of vegetation biomass in the low SLR scenarios are smaller with the higher K_b
524 because the entire domain kept pace with the rate of SLR (see the elevation profiles in Fig. 4b),
525 which resulted in a more uniform biomass distribution across the marsh. However, with the
526 lower K_b, the simulation shows an abrupt decrease when the marshland was submerged in water
527 (Fig. 8d), similar to the final biomass profile in the high SLR scenarios.

528 For the mixed-veg cases, despite the different locations of the abrupt decreases, they
529 showed similar patterns under the lower K_b (Fig. 8c and d), but different responses under the
530 higher K_b (Fig. 8a and b). In the low SLR condition with the higher K_b (Fig. 8b), the mixed
531 vegetation biomass was relatively uniform and greatly exceeded the linear and non-linear single
532 species simulations across the entire model domain (the gray dashed line). In contrast, under the
533 high SLR and higher K_b scenario (Fig. 8a), the mixed vegetation biomass outpaced the single
534 species within ~150 m from the seaward boundary, but then rapidly decreased landward of this
535 location to zero. The Spartina-linear and nonlinear formulations increased approximately

linearly and then decreased to zero at further locations landward, compared with the mixed-veg cases. The Spartina-nonlinear cases showed a higher estimated vegetation biomass than the biomass in the Spartina-linear cases, but the biomass started to decrease to zero closer to the seaward boundary in the Spartina-nonlinear cases, which reflected the nature of the differences in the assumptions in the vegetation equations.

In order to examine the temporal evolution of biomass across the marsh, we plotted the time series at three locations: the seaward boundary, and 100 m and 400 m landward of the boundary (Figure 9). Across the 12 simulation scenarios, the temporal evolution of biomass may be divided into three stages, though not all stages are present at all locations or every scenario.

Rapid change characterizes the first stage. With the exception of mixed vegetation (Figure 9 c, f, i, and l) all locations exhibited rapid increases in biomass for the first 100 to 200 years of the simulation. During the second stage, biomass continued to adjust but at significantly slower rates than the first stage. These adjustments are seen at 100 m in the Spartina linear simulations under both SLR forcings and K_b values (orange circles in Figure a, d, g, and j) and Spartina nonlinear simulations (orange circles in Figure 9b, e, h, and k). A dramatic exception to the gradual adjustments in Stage 2 is the 400 m location in the Spartina-linear and -nonlinear rapid SLR (green circles in Figs 9a, b, d, and e) scenarios and the low K_b scenarios (green circles in Figs. 9d, e, j, and k) in which biomass rapidly drops back to a value of zero between 250 and 350 years.

The third stage is the period when a system enters a stable state or equilibrium state. In all the cases, the vegetation biomass did not change, which indicated that a new equilibrium or quasi-equilibrium state was reached under the new rate of SLR. Examples of this stability

include the limited changes in vegetation biomass near the seaward boundary and at the 100 m locations in all the cases. This is because the vertical accretion rate at these locations in all the cases always kept pace with the rates of SLR.

4.2.2 Parametric sensitivity for vegetation dynamics

After analyzing the spatial and temporal variation of vegetation biomass change, we computed the sensitivity of biomass estimation at the seaward boundary and upland boundary to model parameterization based on the ensemble simulations. The biomass estimations were more sensitive to the vegetation-related parameters, especially the parameters of "maximum organic production rate" and "maximum biomass" (Fig. 10). For the vegetation biomass at the upland (the second, fourth, and sixth columns in Fig. 10a and b), "maximum organic production rate" and "maximum biomass" were the two most dominant parameters that control the estimation of biomass. However, the vegetation biomass near the seaward boundary was also sensitive to sediment settling-related parameters. Specifically, in the high SLR scenario, the biomass estimations near the seaward boundary (the first, third, and fifth columns in Fig. 10a) were also sensitive to all the other parameters, except the parameters for erosion (e.g., "erosion coefficient"). In contrast, in the low SLR scenario, the most sensitive sediment settling-related parameters were only "sediment concentration" and "settling velocity" in the Spartina-dominant cases (the first and third columns in Fig. 10b). The vegetation biomass estimation near the seaward boundary in the mixed-veg case was more sensitive to "maximum biomass" and "maximum organic production rate" than the rest parameters. The values of sensitivity for each parameter in each scenario can be found in Tables S5 and S6.

5 Discussion

5.1 Coastal marsh vulnerability under accelerating SLR

5.1.1 Will coastal marsh survive under future SLR?

Our numerical experiments examined the spatial and temporal variation of coastal marsh evolution under three different representations of vegetation dynamic processes. The results presented similar features of final elevation profiles under the three vegetation schemes: 1) the elevation near the seaward boundary kept pace with both the high and low SLR rates (e.g., 0.005m/yr and 0.01m/yr) and the high and low K_b, even with a conservative sediment concentration (e.g., C_0=20 mg/L) at the seaward boundary (Fig. 4) and 2) the elevation landward declined and part of it drowned in water for the high SLR scenarios and low SLR with low K_b. The elevation near the seaward boundary started to approach a new equilibrium state under the rising SL conditions around 100 years (e.g., the cyan circles in Fig. 9a, b, d, e, g, h, j, and k), which was consistent with the findings in previous studies (D'Alpaos et al., 2011; Kirwan, Temmerman, et al., 2016; Kirwan & Temmerman, 2009; Temmerman et al., 2003; van Wijnen & Bakker, 2001). This pattern of lower accretion rates in the interior of marshes has been previously documented in both modeling (D'Alpaos et al., 2019; Marani et al., 2013; Ratliff et al., 2015) and field studies (Palinkas & Engelhardt, 2019).

Under climate change, if the maximum organic soil production rate (K_b) increases to a similar level as the rate (0.009 m/yr) used in this study due to the increase of temperature and CO_2 in the future , the spatial and temporal variations of vegetation biomass are relatively small and vary within the vegetation growth range (Figs. 8b and 9g, h, and i) under the lower SLR rate (0.005m/yr). Based on these results, a SLR of 0.005m/yr does not appear to threaten the

survival of coastal marsh systems characterized by these types of vegetation on a 500-year scale. However, for a K_b rate commonly observed today (0.003m/yr), all the SLR scenarios showed clear declines of surface elevation starting near the middle or upper of the domain (solid lines in Fig. 4a) and continuing to the upland boundary illustrating that the accretion rate at the inland portion of the coastal marsh cannot keep pace with the high SLR. These inland areas turned into open water habitats with degradation and marsh vegetation mortality occurring after 200-300 years in these locations (Figs. 8a and 9a and b), which may lead to the change of coastal marsh ecosystem functions and hydrological regime shift (Ganju et al., 2020).

The simulations above used a conservative sediment concentration rate from the ocean boundary (C_0=20 mg/L), which limited the delivery of sediment landward under the high SLR rate, resulting the drowning of upland marsh. However, in our simulation with a higher sediment concentration from the ocean (C_0=100 mg/L), more sediment entered the domain and improved the potential for survival of coastal marshland under high SLR. However, simulations with the higher sediment concentration delayed, but didn't prevent upland submergence, which further demonstrated that coastal marsh is largely vulnerable under the high rate of SLR (0.01 m/yr) (see Figs. S2 and S3 in the supplementary information). Also, we assumed a closed boundary at the upland. The sediment supply and geomorphologic structure of the upland area can be an important factor to maintain the accretion rate of high marsh (Kirwan, Walters, et al., 2016; Yousefi Lalimi et al., 2020), which is worth further exploring in a future study.

5.1.2 Marsh vulnerability due to vegetation representation

The experimental cases with different vegetation schemes consistently predicted coastal marsh vulnerability under future SLR. Under a conservative sediment concentration from the ocean (C_0=20 mg/L), at the seaward boundary, marsh elevation accretion should keep pace with

future SLR, regardless the rate of SLR and K_b values. Landward, the inland part of the coastal marsh was resilient under low rate of SLR (0.005m/yr) and simultaneously with the higher K_b, but potentially vulnerable to collapse under high rate of SLR or with the lower K_b.

Our simulations also highlighted marsh response to increased ponded water depth under future SLR. The mixed-veg scheme was the most resilient scenario under the lower SLR and with the higher K_b (gray solid line in Fig. 4b): the marsh accretion rate exceeded the SLR rate throughout the entire domain due to less inundation condition and high organic soil production rate. However, the mixed-veg scheme was the most vulnerable scenario under the higher SLR or with the lower K_b (gray solid line in Figs. 4a, c, and d): the decline of marsh elevation started within ~150 m of the seaward boundary due to a high inundation condition under the higher SLR scenario and lower organic soil production rate. Except for the mixed-veg case under the lower SLR, the Spartina-nonlinear cases predicted larger elevation increases throughout the domain and less elevation depression (Fig. 4) due to a higher vegetation biomass and its associated organic soil production rate (Fig.8). However, the vegetation biomass started to decrease closer to the seaward boundary in the Spartina-nonlinear case, compared with the Spartina-linear case, which implies that the Spartina-nonlinear case predicted a higher unvegetated-vegetated marsh ratio (UVVR) as defined in *Ganju et al. (2017)*.

In addition, our simulation depicted the evolution of vegetation biomass with the evolution of marsh landscape (Fig. 9), reflecting some of the plant life-history traits (Schwarz et al., 2018). The vegetation biomass of our studied marshland varied through different trajectories at the seaward boundary, mid-marshland, and the upland (Fig. 9). In general, vegetation biomass at the seaward boundary and mid-land reached an equilibrium state at around 100-200 years and dropped dramatically at the upland with the drowning of marshland, revealing the

different vegetation responses at different location to boundary drivers and geomorphological change. Notably, the mixed-vegetation scheme predicted that vegetation landward would die out quicker under the high SLR rate (Fig. 9c) than the vegetation in the other vegetation cases. The similarity and distinction of vegetation evolution represented by the different vegetation schemes can potentially describe different vegetation colonization behaviors and cross-species competition during the evolution of coastal marsh (D'Alpaos et al., 2019; Schwarz et al., 2018).

5.2 Implication to data-model integration and future coastal eco-geomorphologic modeling

We found that the "sediment concentration" and "tidal amplitude" are the most sensitive parameters for coastal marsh evolution, which is in agreement with the findings in some prior studies (D'Alpaos et al., 2007; Kirwan, Walters, et al., 2016; Temmerman et al., 2003). More importantly, this study also identified additional parameters that are highly sensitive for the spatial and temporal variations of key landscape characteristics, such as 1) the *Depth_m* (depth between MHTL and marsh elevation at the seaward boundary), 2) elevation relief, 3) averaged sediment fluxes, and 4) vegetation biomass near the seaward boundary and at the upland. These parameters include "sediment diffusivity", "maximum organic production rate", and "maximum biomass". Thus, this sensitivity analysis highlights the need for future modeling and field observations to better measure and parameterize these controls on marsh evolution.

In particular, our sensitivity analysis identified the parameter of "sediment diffusivity" as one of the most sensitive parameters for predicting marshland evolution, especially controlling elevation relief, which implies the importance of hydrodynamic process that brings water and sediment landward and back to ocean. Although the evaluation of coastal hydrodynamics is outside the scope of this study, a good representation of coastal hydrodynamics as a function of coastal boundary condition (e.g., tide and wave), topographic

gradient, and vegetation effect (e.g., influencing surface roughness) is critical for predicting sediment budget accurately and is worth deeper investigation in future modeling studies (Best et al., 2018; Duvall et al., 2019).

Our sensitivity analysis also showed the importance of "maximum biomass" and "organic production rate" for the prediction of marshland elevation changes. Within most of the current eco-geomorphologic models, they are fixed through time. However, future climate changes, higher temperature and CO_2 conditions might change the value of these parameters. For example, the high CO_2 might result in a higher maximum biomass due to the CO_2 fertilization effects (Langley et al., 2009; Ratliff et al., 2015) and high temperature can lead to higher decomposition rates and thus a lower organic production rate (Crosby et al., 2017). Therefore, to improve the prediction accuracy, it is critical to have process-based models that can incorporate the impact of future climates on vegetation production and litter decomposition.

5.3 Representativeness and uncertainty

In this study, we selected the parameter values and the rates of SLR that were widely used in previous modeling studies or were established in the literature from field measurements to ensure that the simulations were realistic and representative. Additionally, the formulations used to represent the dominant processes were selected from broadly used sedimentation, erosion, and vegetation dynamic equations. Thus, the individual simulations should reflect current model capabilities and formulations used to understand process interactions and marsh response to SLR. Based on the ensemble simulations, we generated a large number of parameter samples for the sensitivity analysis. Thus, the results of the sensitivity analyses reasonably reflected the overall sensitivity of the model processes over their physical parameter ranges. The representativeness of the D-model simulations for eco-geomorphic evolution was

694 also supported by simulations from the M-model (see associated results and parametric
695 sensitivity in Figures. S4 to S8 supplementary information). Both sets of simulations from each
696 model had consistent elevation profiles under different rates of SLR and Spartina-nonlinear
697 scheme (M-model only uses the Spartina-nonlinear scheme) and identified similar most
698 sensitive parameters.

699 The models used a no-flow boundary condition at the upland boundary, which limits the
700 water and sediment supply from uplands through upland surface and subsurface environments.
701 An appropriate consideration of the hydrologic and geomorphologic connectivity with the
702 upland region may improve the flexibility of our test model in realistically representing a wider
703 variety of settings, in terms of the relevant hydrodynamic and sediment transport processes
704 (Wohl et al., 2019; Zhang et al., 2018), especially for intertidal areas receiving water and
705 sediment from both riverine and ocean sources (Gleichauf et al., 2014; Wolfram et al., 2016;
706 Yousefi Lalimi et al., 2020). At the seaward boundary, the models used constant sediment
707 concentration in rivers/ocean, while variability in this concentration could contribute to the
708 uncertainty in predictions of the accretion rate on coastal marshes. In addition, a more precise
709 estimation of sediment concentration in the aquatic systems by using high resolution field
710 measurements or a high-resolution, process-based coastal ocean model would improve the
711 predictive capability of coastal marsh eco-geomorphologic models (Stumpf, 1983; Temmerman
712 et al., 2003).

713 **6 Conclusion**

714 We used a coastal eco-geomorphologic model with different vegetation dynamic
715 representations to investigate eco-geomorphologic feedbacks on the coastal marsh and changes
716 in model parametric sensitivity under various future SLR conditions. We conducted model

717 simulations by using a standard set of test cases with consistent model settings and parameters.
718 This study explored coastal marsh evolution under SLR not only from the domain averaged
719 features, but also from the spatial and temporal variations of key landscape characteristics, such
720 as the elevation relief and biomass at the seaward boundary and upland. We found that
721 evaluating the spatial and temporal coastal marsh evolution under different representations of
722 vegetation dynamic process provides new insights to better understanding the uncertainty of
723 predicting coastal marshes vulnerability facing future accelerating SLR from different process
724 representations.

725 Qualitatively, the three vegetation dynamic schemes (Spartina-linear, Spartina-
726 nonlinear, and mixed vegetation linear equations) produce consistent evaluations of the
727 vulnerability of the coastal marsh under high and low SLR rates. However, the Spartina-
728 nonlinear scheme predicted the highest vegetation biomass and organic production rate,
729 yielding the highest accretion rate and elevation, except for the mixed-veg case under the low
730 SLR. The mixed-veg case represents the most resilient marsh type under low SLR with high K_b,
731 but is the most vulnerable case under high SLR. Except the mixed-veg case under the low SLR,
732 all the Spartina-linear cases predicted the largest marsh extent and smallest open water area.

733 The sensitivity analysis study identified the parameters whose values most critically
734 affect model outcomes under different SLR conditions. The parametric sensitivity of the eco-
735 geomorphologic models (e.g., the D- and M-model used in this study) were not the same under
736 the high and low SLR conditions. For example, the most sensitive parameter, such as the
737 maximum organic production rate, in the simulation under the high SLR, was not the most
738 sensitive parameter in the low SLR scenario. The differences in parametric sensitivity
739 highlighted the importance of evaluating parametric sensitivity under different external drivers.

740 The findings in this study provide new insights into how to appropriately model key
741 processes in different coastal marsh landscapes under SLR and vegetation evolution, which has
742 practical consequences for coastal ecosystem management and protection. The sensitivity
743 analysis identified key parameters under different climate change conditions, which serves to
744 inform future field measurements and modeling studies.

745 **Acknowledgments**

746 We thank the constructive comments from the three anonymous reviewers. The research
747 presented in this paper was supported by the Laboratory Direct Research and Development
748 program at Los Alamos National Laboratory under project number 20180033DR. This research
749 used resources provided by the Los Alamos National Laboratory Institutional Computing
750 Program, which is supported by the U.S. Department of Energy National Nuclear Security
751 Administration under Contract No. 89233218CNA000001. MM and AD acknowledge support
752 by Provveditorato for the Public Works of Veneto, Trentino Alto Adige, and Friuli Venezia
753 Giulia, provided through the concessionary of State Consorzio Venezia Nuova and coordinated
754 by CORILA in the framework of the Venezia 2021 Research Program

755 This study is a model-based study that uses two numerical models and synthetic
756 experiments. The model source code are available in the model repositories from the
757 Community Surface Dynamics Modeling System (CSDMS)
758 https://csdms.colorado.edu/wiki/Model_download_portal. Model parameters are listed in the
759 tables above.

References

Allen, J. R. (1995). Salt-marsh growth and fluctuating sea level: implications of a simulation model for Flandrian coastal stratigraphy and peat-based sea-level curves. *Sedimentary Geology*, *100*(1–4), 21–45.

Allen, J. R. (2000). Morphodynamics of Holocene salt marshes: a review sketch from the Atlantic and Southern North Sea coasts of Europe. *Quaternary Science Reviews*, *19*(12), 1155–1231.

Barbier, E. B., Hacker, S. D., Kennedy, C., Koch, E. W., Stier, A. C., & Silliman, B. R. (2011). The value of estuarine and coastal ecosystem services. *Ecological Monographs*, *81*(2), 169–193. https://doi.org/10.1890/10-1510.1

Belliard, J.-P., Toffolon, M., Carniello, L., & D'Alpaos, A. (2015). An ecogeomorphic model of tidal channel initiation and elaboration in progressive marsh accretional contexts. *Journal of Geophysical Research: Earth Surface*, *120*(6), 1040–1064. https://doi.org/10.1002/2015JF003445

Best, Ü. S. N., Van der Wegen, M., Dijkstra, J., Willemsen, P. W. J. M., Borsje, B. W., & Roelvink, D. J. A. (2018). Do salt marshes survive sea level rise? Modelling wave action, morphodynamics and vegetation dynamics. *Environmental Modelling & Software*, *109*, 152–166. https://doi.org/10.1016/j.envsoft.2018.08.004

Brush Jr., L. M. (2012). Exploratory study of sediment diffusion. *Journal of Geophysical Research (1896-1977)*, 1427–1433. https://doi.org/10.1029/JZ067i004p01427@10.1002/(ISSN)2156-2202.EROSIO1

Burkett, V., & Kusler, J. (2000). CLIMATE CHANGE: POTENTIAL IMPACTS AND INTERACTIONS IN WETLANDS OF THE UNTTED STATES.

Cahoon, D. R., & Guntenspergen, G. R. (2010). Climate change, sea-level rise, and coastal wetlands. *National Wetlands Newsletter*, *32*(1), 8–12.

Cao, Z., Wolfram, P., Rowland, J., Zhang, Y., & Pasqualini, D. (2020). Estimating sediment settling velocities from a theoretically-guided, data-driven approach. *Journal of Hydraulic Engineering*. https://doi.org/10.1061/(ASCE)HY.1943-7900.0001798

Carniello, L., Defina, A., Fagherazzi, S., & D'Alpaos, L. (2005). A combined wind wave–tidal model for the Venice lagoon, Italy. *Journal of Geophysical Research: Earth Surface*, *110*(F4).

Carus, J., Paul, M., & Schröder, B. (2016). Vegetation as self-adaptive coastal protection: Reduction of current velocity and morphologic plasticity of a brackish marsh pioneer. *Ecology and Evolution*, *6*(6), 1579–1589. https://doi.org/10.1002/ece3.1904

788 Costanza, R., d'Arge, R., de Groot, R., Farber, S., Grasso, M., Hannon, B., et al. (1997). The value of the world's
789 ecosystem services and natural capital. *Nature*, *387*(6630), 253–260. https://doi.org/10.1038/387253a0
790 Crosby, S. C., Angermeyer, A., Adler, J. M., Bertness, M. D., Deegan, L. A., Sibinga, N., & Leslie, H. M. (2017).
791 Spartina alterniflora Biomass Allocation and Temperature: Implications for Salt Marsh Persistence with
792 Sea-Level Rise. *Estuaries and Coasts*, *40*(1), 213–223. https://doi.org/10.1007/s12237-016-0142-9
793 Cukier, R., Fortuin, C., Shuler, K. E., Petschek, A., & Schaibly, J. (1973). Study of the sensitivity of coupled
794 reaction systems to uncertainties in rate coefficients. I Theory. *The Journal of Chemical Physics*, *59*(8),
795 3873–3878.
796 Da Lio, C., D'Alpaos, A., & Marani, M. (2013). The secret gardener: vegetation and the emergence of
797 biogeomorphic patterns in tidal environments. *Philosophical Transactions of the Royal Society A:*
798 *Mathematical, Physical and Engineering Sciences*, *371*(2004), 20120367.
799 D'Alpaos, A., & Marani, M. (2016). Reading the signatures of biologic–geomorphic feedbacks in salt-marsh
800 landscapes. *Advances in Water Resources*, *93*, 265–275. https://doi.org/10.1016/j.advwatres.2015.09.004
801 D'Alpaos, A., Marani, M., & Rinaldo, A. (2007). Landscape evolution in tidal embayments: Modeling the interplay
802 of erosion, sedimentation, and vegetation dynamics. *Journal of Geophysical Research: Earth Surface*,
803 *112*(F1). https://doi.org/10.1029/2006JF000537
804 D'Alpaos, A., Mudd, S. M., & Carniello, L. (2011). Dynamic response of marshes to perturbations in suspended
805 sediment concentrations and rates of relative sea level rise. *Journal of Geophysical Research: Earth*
806 *Surface*, *116*(F4). https://doi.org/10.1029/2011JF002093
807 D'Alpaos, A., Lanzoni, S., Rinaldo, A., & Marani, M. (2019). Chapter 5 - Salt-Marsh Ecogeomorphological
808 Dynamics and Hydrodynamic Circulation. In G. M. E. Perillo, E. Wolanski, D. R. Cahoon, & C. S.
809 Hopkinson (Eds.), *Coastal Wetlands* (pp. 189–220). Elsevier. https://doi.org/10.1016/B978-0-444-63893-
810 9.00005-8
811 Danielson, J. J., Poppenga, S. K., Brock, J. C., Evans, G. A., Tyler, D. J., Gesch, D. B., et al. (2016).
812 Topobathymetric Elevation Model Development using a New Methodology: Coastal National Elevation
813 Database. *Journal of Coastal Research*, *76*, 75–89. https://doi.org/10.2112/SI76-008

Day, J. W., Christian, R. R., Boesch, D. M., Yáñez-Arancibia, A., Morris, J., Twilley, R. R., et al. (2008). Consequences of climate change on the ecogeomorphology of coastal wetlands. *Estuaries and Coasts*, *31*(3), 477–491.

Duvall, M., Wiberg, P., & Kirwan, M. (2019). Controls on Sediment Suspension, Flux, and Marsh Deposition near a Bay-Marsh Boundary. *Estuaries and Coasts*, *42*(2), 403–424. https://doi.org/10.1007/s12237-018-0478-4

Fagherazzi, S., Kirwan, M., Mudd, S. M., Guntenspergen, G. R., Temmerman, S., D'Alpaos, A., et al. (2012). Numerical models of salt marsh evolution: Ecological, geomorphic, and climatic factors. *Reviews of Geophysics*, *50*(1).

FitzGerald, D. M., & Hughes, Z. (2019). Marsh Processes and Their Response to Climate Change and Sea-Level Rise. *Annual Review of Earth and Planetary Sciences*, *47*(1), 481–517. https://doi.org/10.1146/annurev-earth-082517-010255

French. (1993). Numerical simulation of vertical marsh growth and adjustment to accelerated sea-level rise, North Norfolk, UK. *Earth Surface Processes and Landforms*, *18*(1), 63–81.

French. (2006). Tidal marsh sedimentation and resilience to environmental change: Exploratory modelling of tidal, sea-level and sediment supply forcing in predominantly allochthonous systems. *Marine Geology*, *235*(1), 119–136. https://doi.org/10.1016/j.margeo.2006.10.009

Ganju, N. K., Defne, Z., Kirwan, M. L., Fagherazzi, S., D'Alpaos, A., & Carniello, L. (2017). Spatially integrative metrics reveal hidden vulnerability of microtidal salt marshes. *Nature Communications*, *8*(1), 14156. https://doi.org/10.1038/ncomms14156

Ganju, N. K., Defne, Z., & Fagherazzi, S. (2020). Are Elevation and Open-Water Conversion of Salt Marshes Connected? *Geophysical Research Letters*, *47*(3), e2019GL086703. https://doi.org/10.1029/2019GL086703

Ghisalberti, M., & Nepf, H. (2005). Mass transport in vegetated shear flows. *Environmental Fluid Mechanics*, *5*(6), 527–551.

Gleichauf, K. T., Wolfram, P. J., Monsen, N. E., Fringer, O. B., & Monismith, S. G. (2014). Dispersion mechanisms of a tidal river junction in the Sacramento–San Joaquin Delta, California. *San Francisco Estuary and Watershed Science*, *12*(LA-UR-14-29557).

Kirwan, M., & Murray, A. B. (2007). A coupled geomorphic and ecological model of tidal marsh evolution. *Proceedings of the National Academy of Sciences*, *104*(15), 6118–6122. https://doi.org/10.1073/pnas.0700958104

Kirwan, M., & Temmerman, S. (2009). Coastal marsh response to historical and future sea-level acceleration. *Quaternary Science Reviews*, *28*(17), 1801–1808. https://doi.org/10.1016/j.quascirev.2009.02.022

Kirwan, M., Guntenspergen, G. R., D'Alpaos, A., Morris, J. T., Mudd, S. M., & Temmerman, S. (2010). Limits on the adaptability of coastal marshes to rising sea level. *Geophysical Research Letters*, *37*(23). https://doi.org/10.1029/2010GL045489

Kirwan, M., Temmerman, S., Skeehan, E. E., Guntenspergen, G. R., & Fagherazzi, S. (2016). Overestimation of marsh vulnerability to sea level rise. *Nature Climate Change*, *6*(3), 253–260. https://doi.org/10.1038/nclimate2909

Kirwan, M., Walters, D. C., Reay, W. G., & Carr, J. A. (2016). Sea level driven marsh expansion in a coupled model of marsh erosion and migration. *Geophysical Research Letters*, *43*(9), 4366–4373. https://doi.org/10.1002/2016GL068507

Krone, R. B. (1962). Flume studies of transport of sediment in estrarial shoaling processes. *Final Report, Hydr.Engr.and Samitary Engr.Res.Lab., Univ.of California*. Retrieved from https://ci.nii.ac.jp/naid/10004496634/

Langley, J. A., McKee, K. L., Cahoon, D. R., Cherry, J. A., & Megonigal, J. P. (2009). Elevated CO2 stimulates marsh elevation gain, counterbalancing sea-level rise. *Proceedings of the National Academy of Sciences*, *106*(15), 6182–6186.

Lesser, G., Roelvink, J., Van Kester, J., & Stelling, G. (2004). Development and validation of a three-dimensional morphological model. *Coastal Engineering*, *51*(8), 883–915.

Marani, M., Lanzoni, S., Silvestri, S., & Rinaldo, A. (2004). Tidal landforms, patterns of halophytic vegetation and the fate of the lagoon of Venice. *Journal of Marine Systems*, *51*(1), 191–210. https://doi.org/10.1016/j.jmarsys.2004.05.012

Marani, M., D'Alpaos, A., Lanzoni, S., Carniello, L., & Rinaldo, A. (2007). Biologically-controlled multiple equilibria of tidal landforms and the fate of the Venice lagoon. *Geophysical Research Letters*, *34*(11).

867 Marani, M., D'Alpaos, A., Lanzoni, S., Carniello, L., & Rinaldo, A. (2010). The importance of being coupled:
868 Stable states and catastrophic shifts in tidal biomorphodynamics. *Journal of Geophysical Research: Earth*
869 *Surface, 115*(F4).
870 Marani, M., Da Lio, C., & D'Alpaos, A. (2013). Vegetation engineers marsh morphology through multiple
871 competing stable states. *Proceedings of the National Academy of Sciences, 110*(9), 3259–3263.
872 Mariotti, G., & Fagherazzi, S. (2010). A numerical model for the coupled long-term evolution of salt marshes and
873 tidal flats. *Journal of Geophysical Research: Earth Surface*, *115*(F1).
874 https://doi.org/10.1029/2009JF001326
875 Moller, I., Kudella, M., Rupprecht, F., Spencer, T., Paul, M., van Wesenbeeck, B. K., et al. (2014). Wave
876 attenuation over coastal salt marshes under storm surge conditions. *Nature Geoscience*, *7*(10), 727–731.
877 https://doi.org/10.1038/ngeo2251
878 Morris, J. T. (2006). Competition among marsh macrophytes by means of geomorphological displacement in the
879 intertidal zone. *Estuarine, Coastal and Shelf Science*, *69*(3–4), 395–402.
880 Morris, J. T., & Bowden, W. B. (1986). A Mechanistic, Numerical Model of Sedimentation, Mineralization, and
881 Decomposition for Marsh Sediments. *Soil Science Society of America Journal*, *50*(1), 96–105.
882 https://doi.org/10.2136/sssaj1986.03615995005000010019x
883 Morris, J. T., Sundareshwar, P., Nietch, C. T., Kjerfve, B., & Cahoon, D. R. (2002). Responses of coastal wetlands
884 to rising sea level. *Ecology*, *83*(10), 2869–2877.
885 Mudd, S. M., Fagherazzi, S., Morris, J. T., & Furbish, D. J. (2004). Flow, sedimentation, and biomass production on
886 a vegetated salt marsh in South Carolina: toward a predictive model of marsh morphologic and ecologic
887 evolution. *The Ecogeomorphology of Tidal Marshes, Coastal Estuarine Stud*, *59*, 165–187.
888 Mudd, S. M., Howell, S. M., & Morris, J. T. (2009). Impact of dynamic feedbacks between sedimentation, sea-level
889 rise, and biomass production on near-surface marsh stratigraphy and carbon accumulation. *Estuarine,*
890 *Coastal and Shelf Science, 82*(3), 377–389.
891 Mudd, S. M., D'Alpaos, A., & Morris, J. T. (2010). How does vegetation affect sedimentation on tidal marshes?
892 Investigating particle capture and hydrodynamic controls on biologically mediated sedimentation. *Journal*
893 *of Geophysical Research: Earth Surface, 115*(F3). https://doi.org/10.1029/2009JF001566

National Ocean Service. (2018, August 13). Where is the highest tide? Retrieved from https://oceanservice.noaa.gov/facts/highesttide.html#26

Nepf, H. (1999). Drag, turbulence, and diffusion in flow through emergent vegetation. *Water Resources Research*, *35*(2), 479–489.

NOAA. (2001). NOAA tide and water level: Cape May, NJ, Station ID:8536110. Retrieved from https://tidesandcurrents.noaa.gov/stationhome.html?id=8536110

Orson, R., Panageotou, W., & Leatherman, S. P. (1985). Response of tidal salt marshes of the US Atlantic and Gulf coasts to rising sea levels. *Journal of Coastal Research*, 29–37.

Palinkas, C. M., & Engelhardt, K. A. M. (2019). Influence of Inundation and Suspended-Sediment Concentrations on Spatiotemporal Sedimentation Patterns in a Tidal Freshwater Marsh. *Wetlands*, *39*(3), 507–520. https://doi.org/10.1007/s13157-018-1097-3

Palmer, M. R., Nepf, H. M., Pettersson, T. J. R., & Ackerman, J. D. (2004). Observations of particle capture on a cylindrical collector: Implications for particle accumulation and removal in aquatic systems. *Limnology and Oceanography*, *49*(1), 76–85. https://doi.org/10.4319/lo.2004.49.1.0076

Parchure Trimbak M., & Mehta Ashish J. (1985). Erosion of Soft Cohesive Sediment Deposits. *Journal of Hydraulic Engineering*, *111*(10), 1308–1326. https://doi.org/10.1061/(ASCE)0733-9429(1985)111:10(1308)

Randerson, P. (1979). A simulation model of salt-marsh development and plant ecology. *Estuarine and Coastal Land Reclamation and Water Storage*, 48–67.

Ratliff, K. M., Braswell, A. E., & Marani, M. (2015). Spatial response of coastal marshes to increased atmospheric CO2. *Proceedings of the National Academy of Sciences*, *112*(51), 15580–15584. https://doi.org/10.1073/pnas.1516286112

Reed, D. J. (1995). The response of coastal marshes to sea-level rise: Survival or submergence? *Earth Surface Processes and Landforms*, *20*(1), 39–48.

Riazi, A., & Türker, U. (2019). The drag coefficient and settling velocity of natural sediment particles. *Computational Particle Mechanics*, *6*(3), 427–437. https://doi.org/10.1007/s40571-019-00223-6

Rinaldo, A., Fagherazzi, S., Lanzoni, S., Marani, M., & Dietrich, W. E. (1999). Tidal networks: 2. Watershed delineation and comparative network morphology. *Water Resources Research*, *35*(12), 3905–3917. https://doi.org/10.1029/1999wr900237

Roelvink, J. (2006). Coastal morphodynamic evolution techniques. *Coastal Engineering*, *53*(2), 277–287.

Rogers, K., Saintilan, N., & Copeland, C. (2012). Modelling wetland surface elevation dynamics and its application to forecasting the effects of sea-level rise on estuarine wetlands. *Ecological Modelling*, *244*, 148–157. https://doi.org/10.1016/j.ecolmodel.2012.06.014

Roulet, N. (1990). The hydrological role of peat-covered wetlands. *The Canadian Geographer/Le Géographe Canadien*, *34*(1), 82–83.

Scavia, D., Field, J. C., Boesch, D. F., Buddemeier, R. W., Burkett, V., Cayan, D. R., et al. (2002). Climate change impacts on U.S. Coastal and Marine Ecosystems. *Estuaries*, *25*(2), 149–164. https://doi.org/10.1007/BF02691304

Scheidegger, A. (1961). Mathematical models of slope development. *Geological Society of America Bulletin*, *72*(1), 37–50.

Schile, L. M., Callaway, J. C., Morris, J. T., Stralberg, D., Parker, V. T., & Kelly, M. (2014). Modeling Tidal Marsh Distribution with Sea-Level Rise: Evaluating the Role of Vegetation, Sediment, and Upland Habitat in Marsh Resiliency. *PLOS ONE*, *9*(2), e88760. https://doi.org/10.1371/journal.pone.0088760

Schuerch, M., Spencer, T., Temmerman, S., Kirwan, M., Wolff, C., Lincke, D., et al. (2018). Future response of global coastal wetlands to sea-level rise. *Nature*, *561*(7722), 231–234. https://doi.org/10.1038/s41586-018-0476-5

Schwarz, C., Gourgue, O., van Belzen, J., Zhu, Z., Bouma, T. J., van de Koppel, J., et al. (2018). Self-organization of a biogeomorphic landscape controlled by plant life-history traits. *Nature Geoscience*, *11*(9), 672–677. https://doi.org/10.1038/s41561-018-0180-y

Silvestri, S., & Marani, M. (2004). Salt-marsh vegetation and morphology: Basic physiology, modelling and remote sensing observations. *The Ecogeomorphology of Tidal Marshes*, *Coastal Estuarine Stud*, *59*, 5–25.

Silvestri, S., Defina, A., & Marani, M. (2005). Tidal regime, salinity and salt marsh plant zonation. *Estuarine, Coastal and Shelf Science*, *62*(1), 119–130. https://doi.org/10.1016/j.ecss.2004.08.010

947 Song, X., Zhang, J., Zhan, C., Xuan, Y., Ye, M., & Xu, C. (2015). Global sensitivity analysis in hydrological
948 modeling: Review of concepts, methods, theoretical framework, and applications. *Journal of Hydrology*,
949 *523*, 739–757.
950 Spencer, T., Schuerch, M., Nicholls, R. J., Hinkel, J., Lincke, D., Vafeidis, A. T., et al. (2016). Global coastal
951 wetland change under sea-level rise and related stresses: The DIVA Wetland Change Model. *Global and*
952 *Planetary Change*, *139*, 15–30. https://doi.org/10.1016/j.gloplacha.2015.12.018
953 Stralberg, D., Brennan, M., Callaway, J. C., Wood, J. K., Schile, L. M., Jongsomjit, D., et al. (2011). Evaluating
954 Tidal Marsh Sustainability in the Face of Sea-Level Rise: A Hybrid Modeling Approach Applied to San
955 Francisco Bay. *PLOS ONE*, *6*(11), e27388. https://doi.org/10.1371/journal.pone.0027388
956 Stumpf, R. P. (1983). The process of sedimentation on the surface of a salt marsh. *Estuarine, Coastal and Shelf*
957 *Science*, *17*(5), 495–508.
958 Temmerman, S., Govers, G., Meire, P., & Wartel, S. (2003). Modelling long-term tidal marsh growth under
959 changing tidal conditions and suspended sediment concentrations, Scheldt estuary, Belgium. *Marine*
960 *Geology*, *193*(1), 151–169. https://doi.org/10.1016/S0025-3227(02)00642-4
961 Temmerman, S., Bouma, T. J., Govers, G., Wang, Z. B., Vries, M. B. D., & Herman, P. M. J. (2005). Impact of
962 vegetation on flow routing and sedimentation patterns: Three-dimensional modeling for a tidal marsh.
963 *Journal of Geophysical Research: Earth Surface*, *110*(F4). https://doi.org/10.1029/2005JF000301
964 Thompson, C. E. L., Amos, C. L., & Umgiesser, G. (2004). A comparison between fluid shear stress reduction by
965 halophytic plants in Venice Lagoon, Italy and Rustico Bay, Canada—analyses of in situ measurements.
966 *Journal of Marine Systems*, *51*(1), 293–308. https://doi.org/10.1016/j.jmarsys.2004.05.017
967 Tiner, R. W. (2013). *Tidal Wetlands Primer*. University of Massachusetts Press.
968 Van Rijn, L. C. (1993). *Principles of sediment transport in rivers, estuaries and coastal seas* (Vol. 1006). Aqua
969 publications Amsterdam.
970 Vreugdenhil, C. B. (2013). *Numerical methods for shallow-water flow* (Vol. 13). Springer Science & Business
971 Media.
972 van Wijnen, H. J., & Bakker, J. P. (2001). Long-term Surface Elevation Change in Salt Marshes: a Prediction of
973 Marsh Response to Future Sea-Level Rise. *Estuarine, Coastal and Shelf Science*, *52*(3), 381–390.
974 https://doi.org/10.1006/ecss.2000.0744

Wohl, E., Brierley, G., Cadol, D., Coulthard, T. J., Covino, T., Fryirs, K. A., et al. (2019). Connectivity as an emergent property of geomorphic systems. *Earth Surface Processes and Landforms*, *44*(1), 4–26.

Wolfram, P. J., Fringer, O. B., Monsen, N. E., Gleichauf, K. T., Fong, D. A., & Monismith, S. G. (2016). Modeling intrajunction dispersion at a well-mixed tidal river junction. *Journal of Hydraulic Engineering*, *142*(8), 04016019.

Xu, C., & Gertner, G. (2011). Understanding and comparisons of different sampling approaches for the Fourier Amplitudes Sensitivity Test (FAST). *Computational Statistics & Data Analysis*, *55*(1), 184–198.

Xu, C., & Gertner, G. Z. (2008a). A general first-order global sensitivity analysis method. *Reliability Engineering & System Safety*, *93*(7), 1060–1071.

Xu, C., & Gertner, G. Z. (2008b). Uncertainty and sensitivity analysis for models with correlated parameters. *Reliability Engineering & System Safety*, *93*(10), 1563–1573.

Yang, S. L., Shi, B. W., Bouma, T. J., Ysebaert, T., & Luo, X. X. (2012). Wave Attenuation at a Salt Marsh Margin: A Case Study of an Exposed Coast on the Yangtze Estuary. *Estuaries and Coasts*, *35*(1), 169–182. https://doi.org/10.1007/s12237-011-9424-4

Yousefi Lalimi, F., Marani, M., Heffernan, J. B., D'Alpaos, A., & Murray, A. B. (2020). Watershed and ocean controls of salt marsh extent and resilience. *Earth Surface Processes and Landforms*, *n/a*(n/a). https://doi.org/10.1002/esp.4817

Zhang, Y., Slingerland, R., & Duffy, C. (2016). Fully-coupled hydrologic processes for modeling landscape evolution. *Environmental Modelling & Software*, *82*, 89–107.

Zhang, Y., Li, W., Sun, G., Miao, G., Noormets, A., Emanuel, R., & King, J. S. (2018). Understanding coastal wetland hydrology with a new regional scale process-based hydrologic model. *Hydrological Processes*. https://doi.org/10.1002/hyp.13247

1008
1009 Table 1. The numerical experiment cases.

	Spartina-dominant linear function	**Spartina-dominant nonlinear function**	**Mixed species linear function**
High SLR rate (0.01 m/yr) and High K_b (0.009 m/yr)	Case 1	Case 2	Case 3
Low SLR rate (0.005 m/yr) and High K_b (0.009 m/yr)	Case 4	Case 5	Case 6
High SLR rate (0.01 m/yr) and Low K_b (0.003 m/yr)	Case 7	Case 8	Case 9
High SLR rate (0.01 m/yr) and Low K_b (0.003 m/yr)	Case 10	Case 11	Case 12

1010

1011 Table 2. Key hydro-eco-geomorphic parameters used in the two models and parameter ranges used for
1012 sensitivity analysis.

Processes	**Parameter description**	**Symbol in the D model**	**Range**	**Individual simulation**	**References**
Erosion	Erosion coefficient $(\frac{kg}{m^2 s P_a})$	α	[2.00E-09, 4.12E-04]	1.12E-04	(D'Alpaos et al., 2007; Mariotti & Fagherazzi, 2010)

	Critical shear stress for erosion (P_a)	τ_e	[0.03, 2]	0.4	(Thompson et al., 2004)
Sedimentation	Critical shear stress for deposition (P_a)	τ_d	[0.05, 2]	0.1	(Parchure Trimbak M. & Mehta Ashish J., 1985)
	Sediment concentration at seaward boundary ($\frac{mg}{liter}$)	C_0	[1, 800]	20	(Kirwan et al., 2010)
	Suspended sediment diffusivity ($\frac{m^2}{s}$)	Sed_{diff}	[0.005, 1]	0.3	(Brush Jr., 2012)
	Sediment settling velocity ($\frac{m}{s}$)	w_s	[5.00E-05, 6.00E-04]	1.00E-04	(Riazi & Türker, 2019)
	Belowground organic production ($\frac{m}{yr}$)	K_b	[0, 0.0135]	0.003 and 0.009	(Mariotti & Fagherazzi, 2010; Mudd et al., 2009,

					2010)
Forcing	Tidal amplitude (m)	AmpTide	[0.1, 4]	0.8	(National Ocean Service, 2018)
Biomass	Minimum depth between MHTL and land surface (m)	D_{biomin}	[0, 0.1]	0.1	(Morris, 2006)
	Maximum depth between MHTL and land surface (m)	D_{biomax}	[0.8, 0.95]	0.8	(Morris, 2006)
	Maximum biomass $(\frac{g}{m^2})$	B_{max}	[0, 3000]	2000	(Mudd et al., 2004)
Hydro-dynamics	Chezy coefficient $(\frac{m^{0.5}}{s})$	CHI	10	10	(D'Alpaos et al., 2007)
	Maximum water velocity $(\frac{m}{s})$	U_{max}	0.2	0.2	(D'Alpaos et al., 2007)

1013

1014

1015

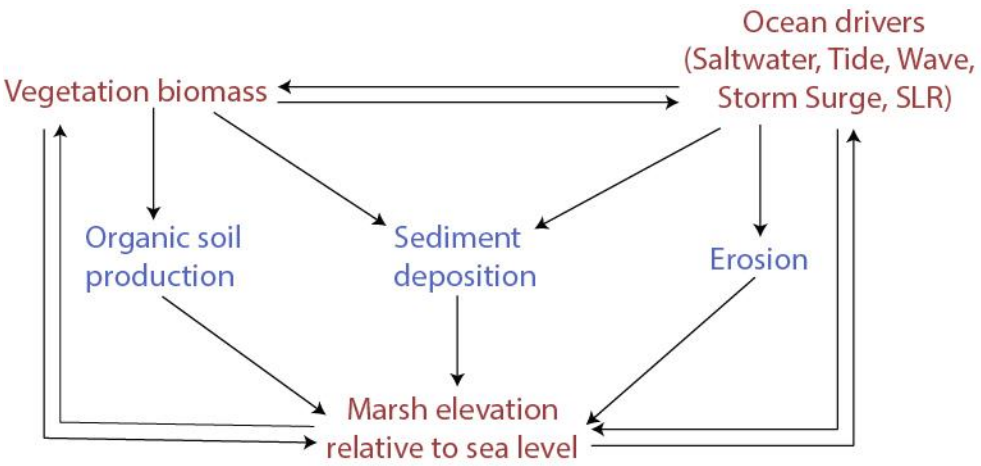

1016

1017 Figure 1. The linkage of hydro-ecogeomorphologic components in coastal marsh systems. The words in
1018 red and blue describe the components and sediment fluxes, respectively.

1019

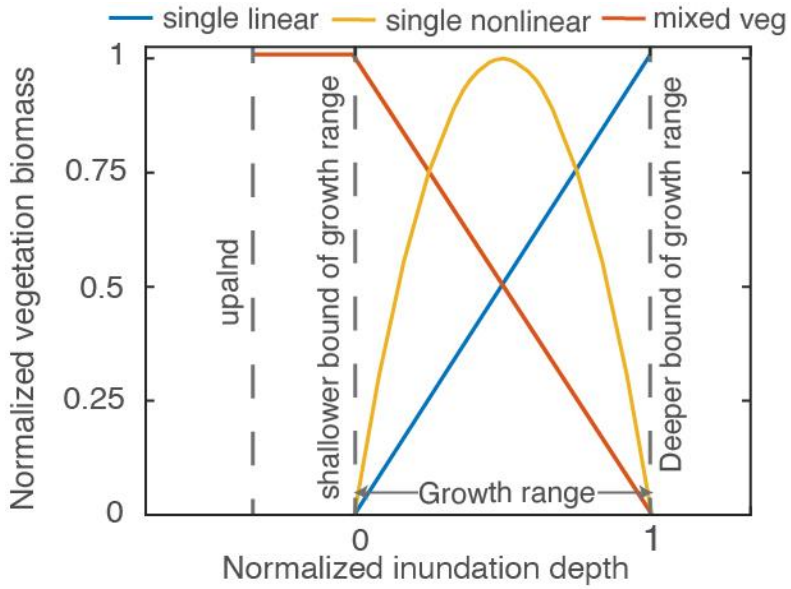

1020

1021 Figure 2 The dynamics of vegetation biomass under different marsh inundation depth normalized by the
1022 vegetation growth range bounded by $MHTL - D_{biomin}$ and $MHTL - D_{biomax}$. $MHTL$ represents the
1023 mean highest tide level. D_{biomax} and D_{biomin} are the highest and lowest inundation depth below MHTL,
1024 respectively.

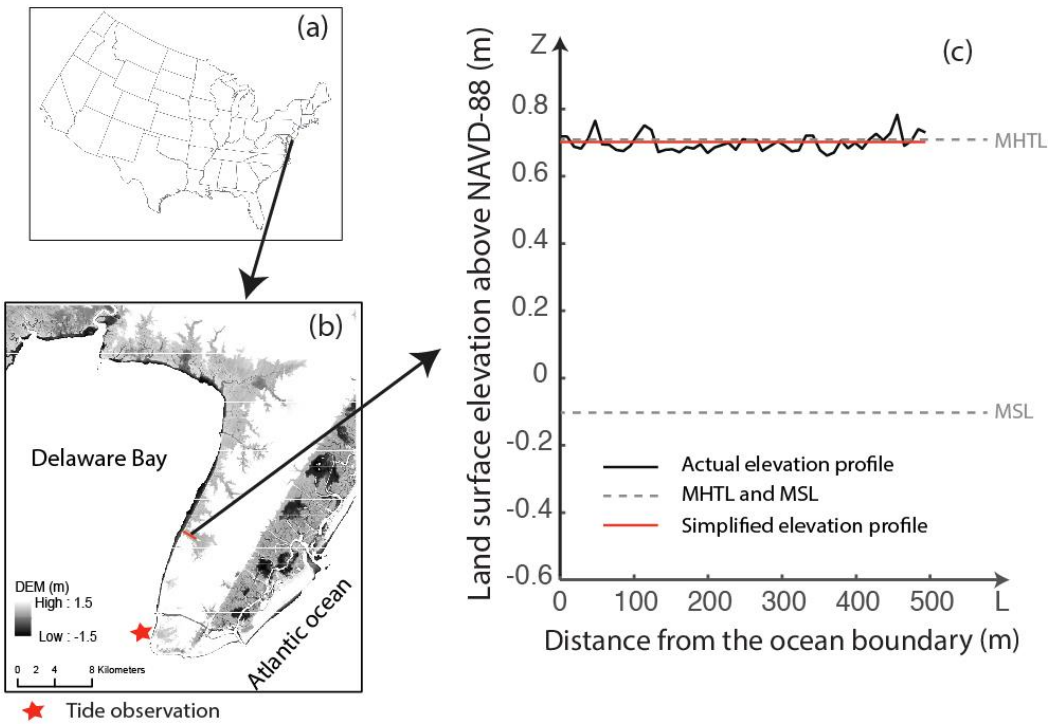

Figure 3 The geographic location and the elevation profile of a 1-D transect at Delaware Bay. (a) and (b) indicate the location of the 1-D transect. The black solid line in (c) shows the actual elevation profile of the 1-D transect. The red line is a simplified elevation profile. The gray dashed lines indicate the MHTL (mean highest tide level) and MSL (mean sea level)

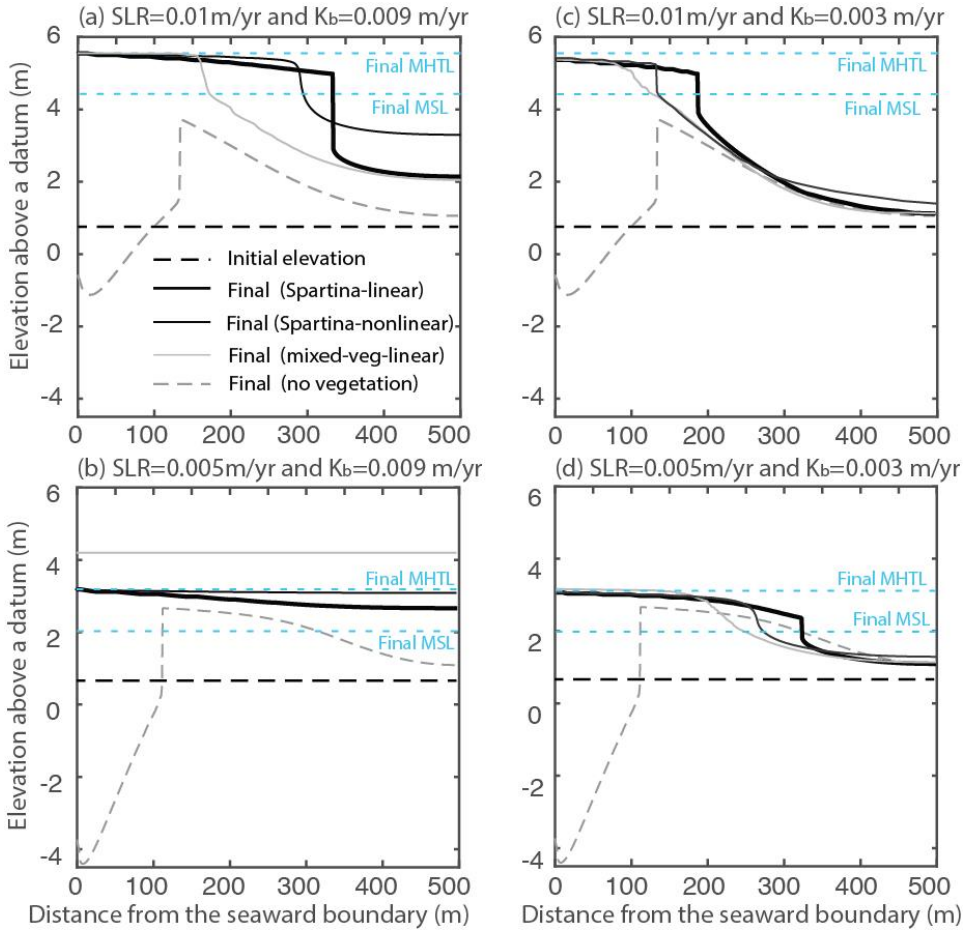

Figure 4. Elevation profiles after 500 years simulation from the seaward boundary (x axis = 0 m) to the upland boundary (x axis = 500 m) for (a) the higher rate of SLR and higher K_b scenario, (b) the lower rate of SLR and higher K_b scenario, (c) the higher rate of SLR and lower K_b scenario, and (d) the lower rate of SLR and lower K_b scenario. The black dashed lines show the initial elevation profile (0.67 m above NAVD88 datum). The thicker and thinner black lines indicate the simulated elevation profiles by using Spartina dominant linear equation and Spartina dominant nonlinear equation, respectively. The gray solid lines are the elevation profiles by using the mixed vegetation linear equation. The gray dashed lines are the simulated elevation profiles without vegetation. The light blue dashed lines indicate the final MHTL and MSL.

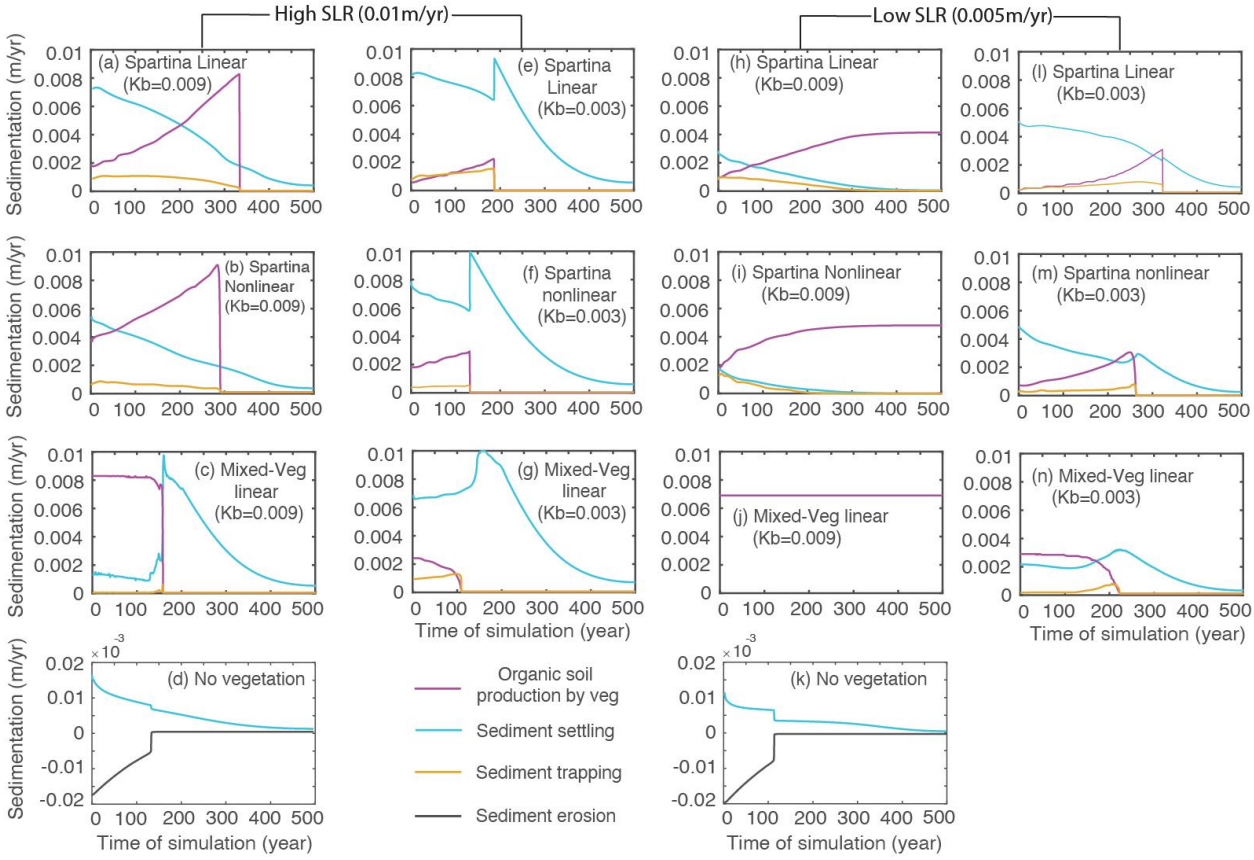

Figure 5. Spatial distribution of the sediment fluxes at the end of 500 years in the D-model simulations. The plots with various colors represent different fluxes in different scenarios.

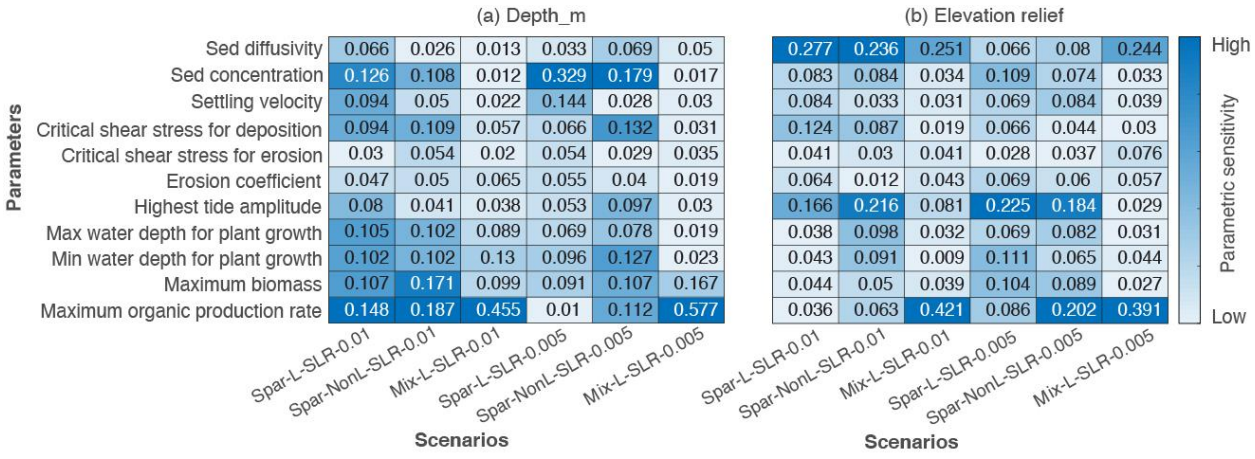

Figure 6. Parametric sensitivity of simulations under (a) high SLR scenario and (b) low SLR scenario. The colors indicate model sensitivity with a high sensitivity coded in dark blue and low sensitivity coded in light blue. The values in each grid represents the sensitivity of the model to the corresponding parameter and simulation case.

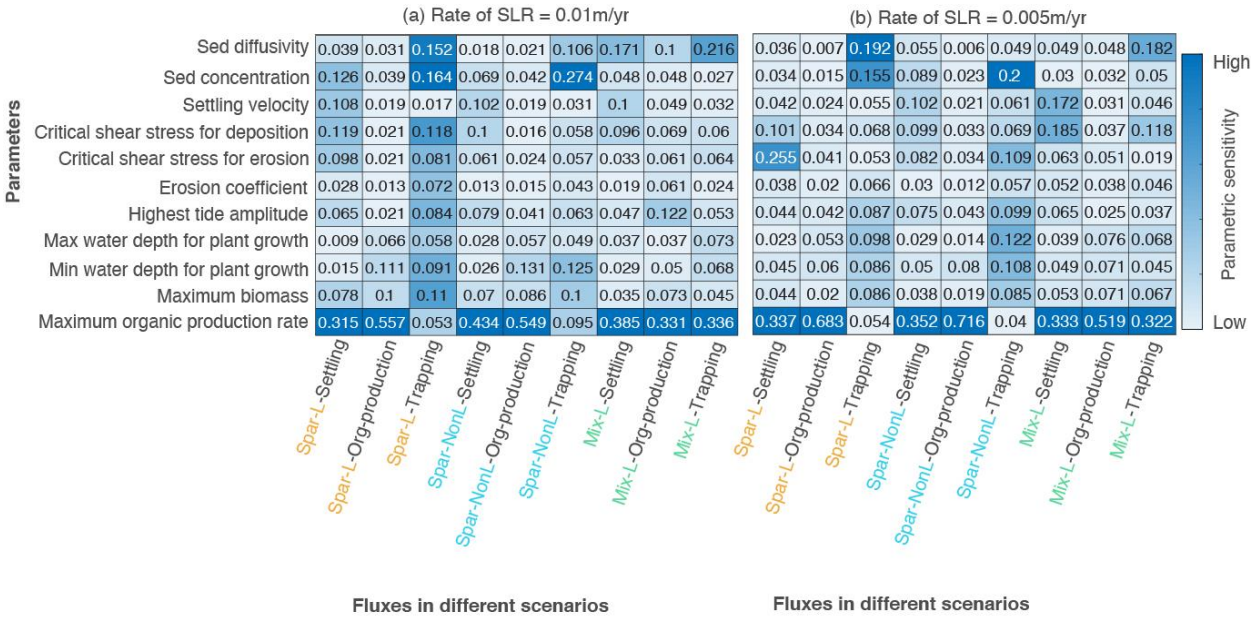

Figure 7. Parametric sensitivity of the sediment fluxes under (a) high SLR scenario and (b) low SLR scenario. The colors indicate model sensitivity with a high sensitivity coded in dark blue and low sensitivity coded in light blue. The value in each grid represents the sensitivity of the model to the corresponding parameter, flux, and simulation case.

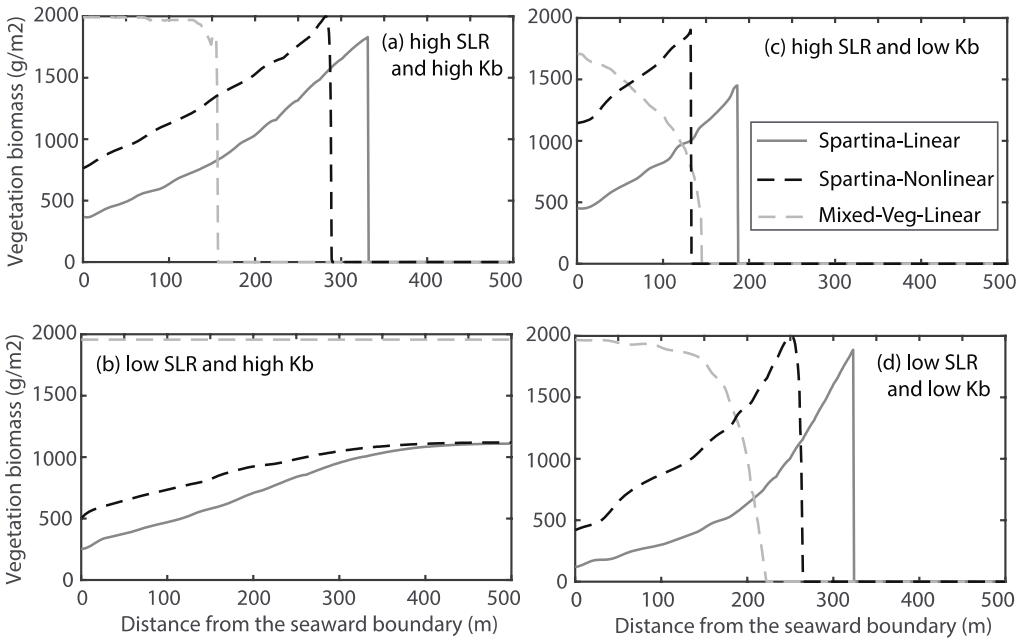

Figure 8. The spatial distribution of vegetation biomass at the end of 500 years throughout the marsh domain under (a) the high SLR and higher K_b scenario, (b) the low SLR and higher K_b scenario, (c) the higher SLR and lower K_b scenario, and (d) the lower SLR and lower K_b scenario.

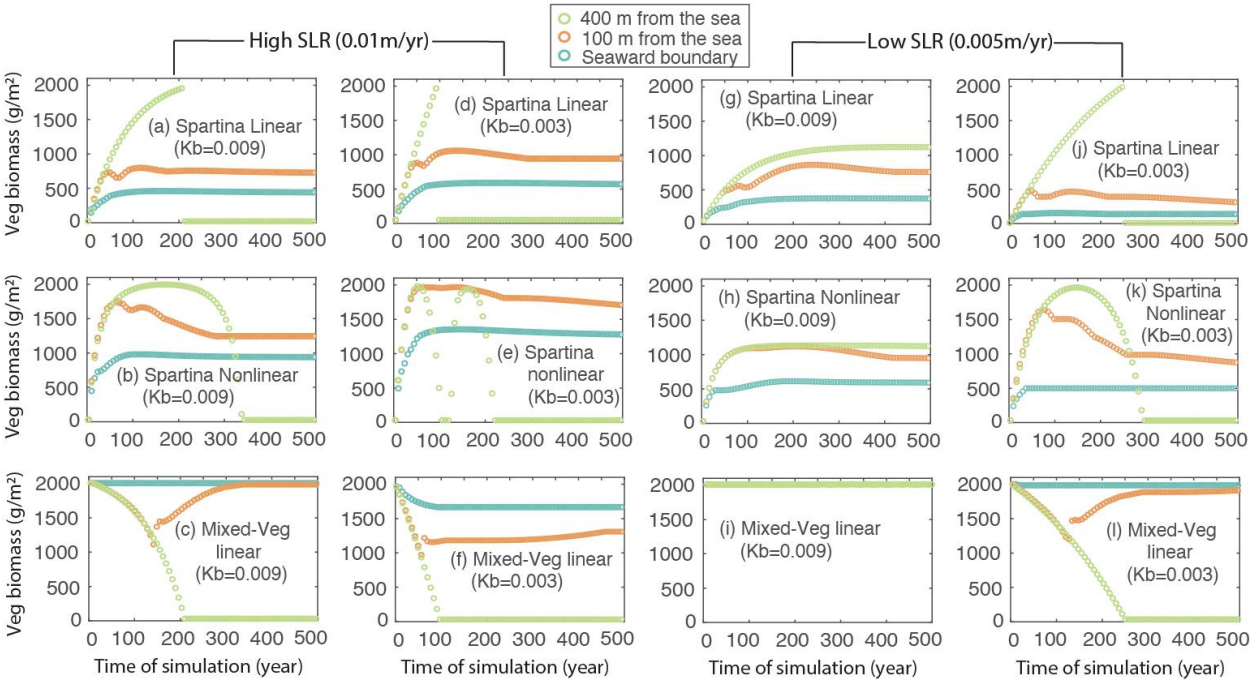

Figure 9. Temporal variation of vegetation biomass for different vegetation cases in different SLR scenarios. The circles in different colors indicate the biomass at different locations of the marsh domain.

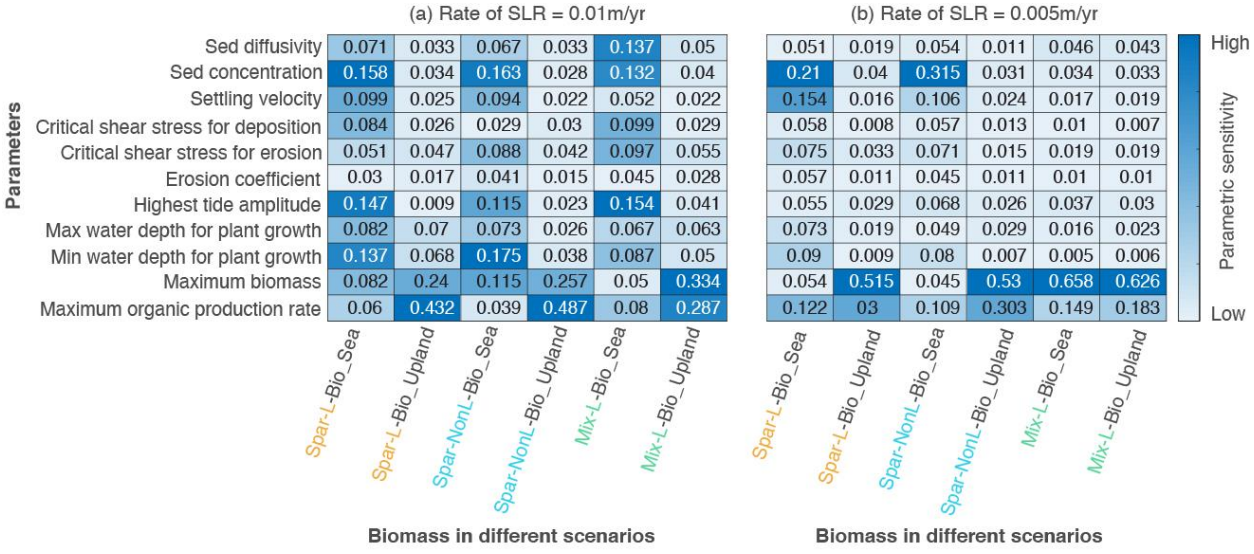

Figure 10. Parametric sensitivity of vegetation biomass under (a) high SLR scenario and (b) low SLR scenario. The colors indicate model sensitivity with a high sensitivity coded in dark blue and low sensitivity coded in light blue. The value in each grid represents the sensitivity of the model to the corresponding parameter, biomass, and simulation case.

Table 1. The numerical experiment cases.

	Spartina-dominant linear function	**Spartina-dominant nonlinear function**	**Mixed species linear function**
High SLR rate (0.01 m/yr) and High K_b (0.009 m/yr)	Case 1	Case 2	Case 3
Low SLR rate (0.005 m/yr) and High K_b (0.009 m/yr)	Case 4	Case 5	Case 6
High SLR rate (0.01 m/yr) and Low K_b (0.003 m/yr)	Case 7	Case 8	Case 9
High SLR rate (0.01 m/yr) and Low K_b (0.003 m/yr)	Case 10	Case 11	Case 12

Table 2. Key hydro-eco-geomorphic parameters used in the two models and parameter ranges used for sensitivity analysis.

Processes	**Parameter description**	**Symbol in the D model**	**Range**	**Individual simulation**	**References**
Erosion	Erosion coefficient $(\frac{kg}{m^2 s P_a})$	α	[2.00E-09, 4.12E-04]	1.12E-04	(D'Alpaos et al., 2007; Mariotti & Fagherazzi, 2010)
	Critical shear stress for erosion (P_a)	τ_e	[0.03, 2]	0.4	(Thompson et al., 2004)
Sedimentation	Critical shear stress for deposition (P_a)	τ_d	[0.05, 2]	0.1	(Parchure Trimbak M. & Mehta Ashish J., 1985)
	Sediment concentration at seaward boundary $(\frac{mg}{liter})$	C_0	[1, 800]	20	(Kirwan et al., 2010)

	Suspended sediment diffusivity ($\frac{m^2}{s}$)	Sed_{diff}	[0.005, 1]	0.3	(Brush Jr., 2012)
	Sediment settling velocity ($\frac{m}{s}$)	w_s	[5.00E-05, 6.00E-04]	1.00E-04	(Riazi & Türker, 2019)
	Belowground organic production ($\frac{m}{yr}$)	K_b	[0, 0.0135]	0.003 and 0.009	(Mariotti & Fagherazzi, 2010; Mudd et al., 2009, 2010)
Forcing	Tidal amplitude (m)	AmpTide	[0.1, 4]	0.8	(National Ocean Service, 2018)
Biomass	Minimum depth between MHTL and land surface (m)	D_{biomin}	[0, 0.1]	0.1	(Morris, 2006)
	Maximum depth between MHTL and land surface (m)	D_{biomax}	[0.8, 0.95]	0.8	(Morris, 2006)
	Maximum biomass ($\frac{g}{m^2}$)	B_{max}	[0, 3000]	2000	(Mudd et al., 2004)

Hydro-dynamics	Chezy coefficient ($\frac{m^{0.5}}{s}$)	CHI	10	10	(D'Alpaos et al., 2007)
	Maximum water velocity ($\frac{m}{s}$)	U_{max}	0.2	0.2	(D'Alpaos et al., 2007)

Figure 1.

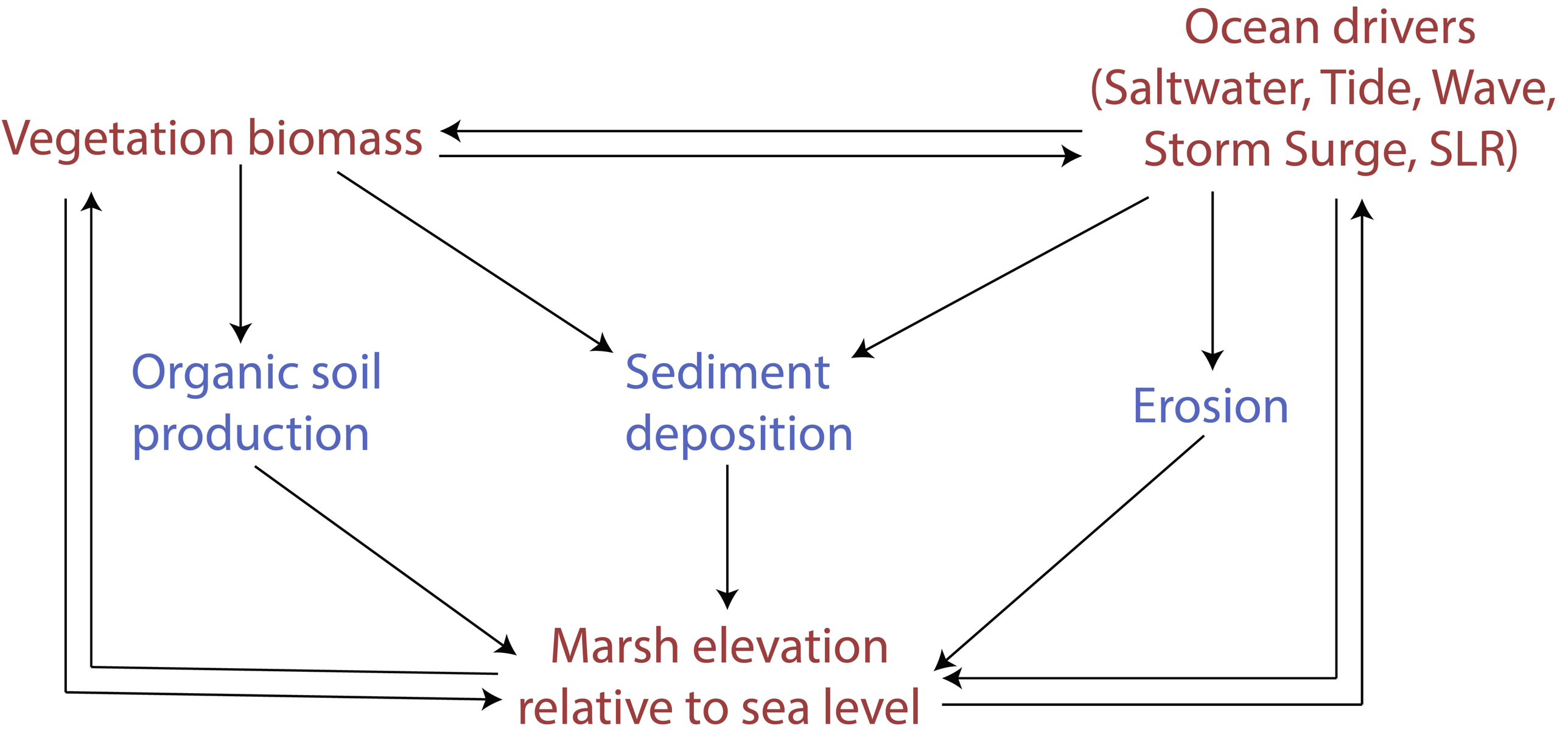
Ocean drivers
(Saltwater, Tide, Wave,
Storm Surge, SLR)
Vegetation biomass
Organic soil
production
Sediment
deposition
Erosion
Marsh elevation
relative to sea level

Figure 2.

single linear
single nonlinear
mixed veg
Normalized vegetation biomass
1
0.75
0.5
0.25
0
upaland
shallower bound of growth range
Deeper bound of growth range
Growth range
0
1
Normalized inundation depth

Figure 3.

(a)

(b)

Delaware Bay

Atlantic ocean

DEM (m)
High : 1.5
Low : -1.5

0 2 4 8 Kilometers

Tide observation

(c)

Land surface elevation above NAVD-88 (m)

Z

0.8
0.6
0.4
0.2
0
-0.2
-0.4
-0.6

MHTL

MSL

Actual elevation profile
MHTL and MSL
Simplified elevation profile

0 100 200 300 400 500 L

Distance from the ocean boundary (m)

Figure 4.

(a) SLR=0.01m/yr and K_b=0.009 m/yr

(b) SLR=0.005m/yr and K_b=0.009 m/yr

(c) SLR=0.01m/yr and K_b=0.003 m/yr

(d) SLR=0.005m/yr and K_b=0.003 m/yr

Final MHTL

Final MSL

Initial elevation

Final (Spartina-linear)

Final (Spartina-nonlinear)

Final (mixed-veg-linear)

Final (no vegetation)

Elevation above a datum (m)

Distance from the seaward boundary (m)

6
4
2
0
-2
-4

0
100
200
300
400
500

Figure 5.

High SLR (0.01m/yr)

Low SLR (0.005m/yr)

Sedimentation (m/yr)

(a) Spartina Linear (Kb=0.009)

(e) Spartina Linear (Kb=0.003)

(h) Spartina Linear (Kb=0.009)

(l) Spartina Linear (Kb=0.003)

(b) Spartina Nonlinear (Kb=0.009)

(f) Spartina nonlinear (Kb=0.003)

(i) Spartina Nonlinear (Kb=0.009)

(m) Spartina nonlinear (Kb=0.003)

(c) Mixed-Veg linear (Kb=0.009)

(g) Mixed-Veg linear (Kb=0.003)

(j) Mixed-Veg linear (Kb=0.009)

(n) Mixed-Veg linear (Kb=0.003)

(d) No vegetation

(k) No vegetation

Time of simulation (year)

Organic soil production by veg

Sediment settling

Sediment trapping

Sediment erosion

Figure 6.

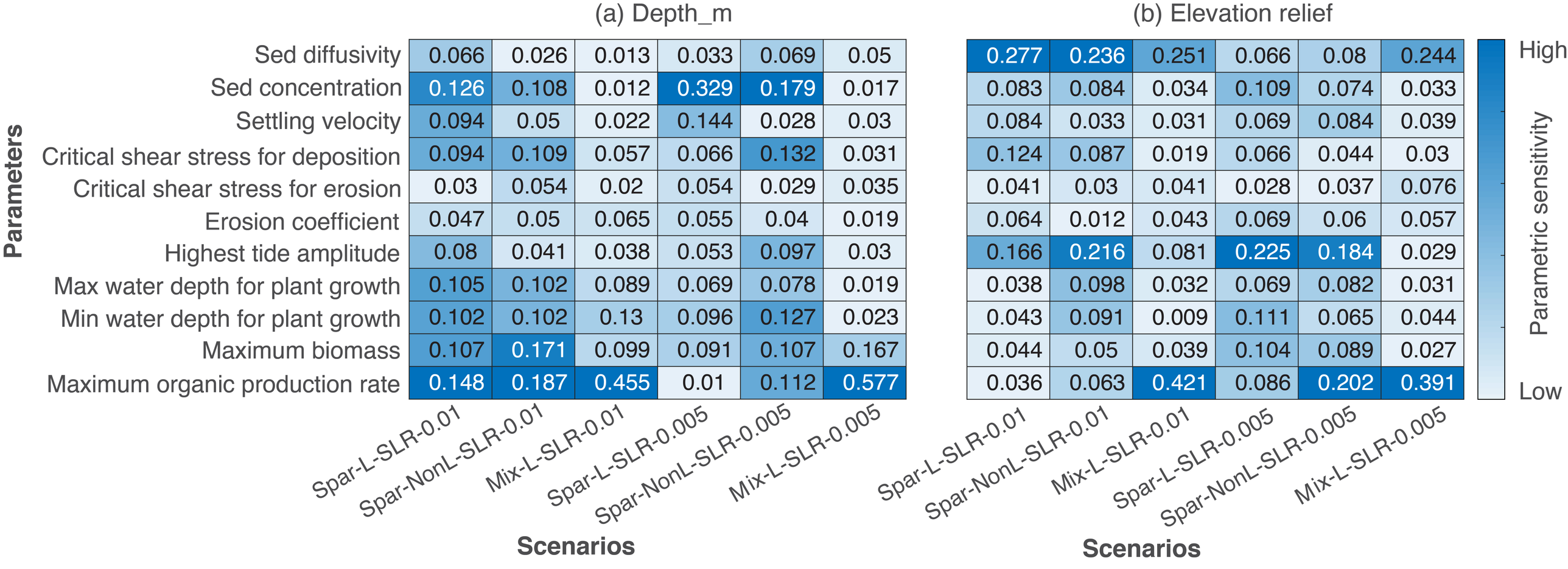
(a) Depth_m
(b) Elevation relief
Parameters
Sed diffusivity
Sed concentration
Settling velocity
Critical shear stress for deposition
Critical shear stress for erosion
Erosion coefficient
Highest tide amplitude
Max water depth for plant growth
Min water depth for plant growth
Maximum biomass
Maximum organic production rate
0.066 0.026 0.013 0.033 0.069 0.05
0.126 0.108 0.012 0.329 0.179 0.017
0.094 0.05 0.022 0.144 0.028 0.03
0.094 0.109 0.057 0.066 0.132 0.031
0.03 0.054 0.02 0.054 0.029 0.035
0.047 0.05 0.065 0.055 0.04 0.019
0.08 0.041 0.038 0.053 0.097 0.03
0.105 0.102 0.089 0.069 0.078 0.019
0.102 0.102 0.13 0.096 0.127 0.023
0.107 0.171 0.099 0.091 0.107 0.167
0.148 0.187 0.455 0.01 0.112 0.577
0.277 0.236 0.251 0.066 0.08 0.244
0.083 0.084 0.034 0.109 0.074 0.033
0.084 0.033 0.031 0.069 0.084 0.039
0.124 0.087 0.019 0.066 0.044 0.03
0.041 0.03 0.041 0.028 0.037 0.076
0.064 0.012 0.043 0.069 0.06 0.057
0.166 0.216 0.081 0.225 0.184 0.029
0.038 0.098 0.032 0.069 0.082 0.031
0.043 0.091 0.009 0.111 0.065 0.044
0.044 0.05 0.039 0.104 0.089 0.027
0.036 0.063 0.421 0.086 0.202 0.391
Spar-L-SLR-0.01
Spar-NonL-SLR-0.01
Mix-L-SLR-0.01
Spar-L-SLR-0.005
Spar-NonL-SLR-0.005
Mix-L-SLR-0.005
Scenarios
Parametric sensitivity
High
Low

Figure 7.

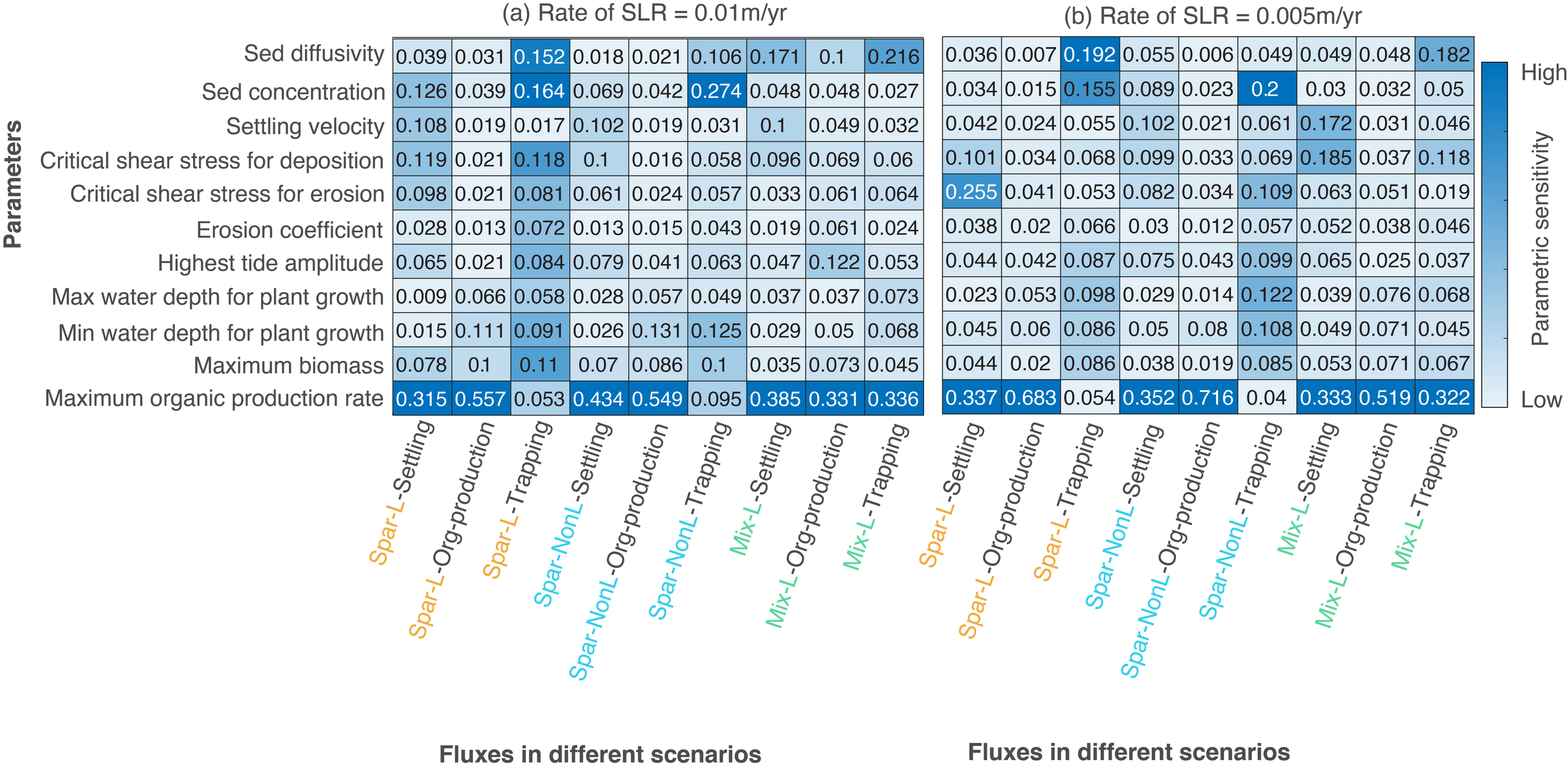
(a) Rate of SLR = 0.01m/yr
(b) Rate of SLR = 0.005m/yr
Parameters
Sed diffusivity
Sed concentration
Settling velocity
Critical shear stress for deposition
Critical shear stress for erosion
Erosion coefficient
Highest tide amplitude
Max water depth for plant growth
Min water depth for plant growth
Maximum biomass
Maximum organic production rate
0.039 0.031 0.152 0.018 0.021 0.106 0.171 0.1 0.216
0.126 0.039 0.164 0.069 0.042 0.274 0.048 0.048 0.027
0.108 0.019 0.017 0.102 0.019 0.031 0.1 0.049 0.032
0.119 0.021 0.118 0.1 0.016 0.058 0.096 0.069 0.06
0.098 0.021 0.081 0.061 0.024 0.057 0.033 0.061 0.064
0.028 0.013 0.072 0.013 0.015 0.043 0.019 0.061 0.024
0.065 0.021 0.084 0.079 0.041 0.063 0.047 0.122 0.053
0.009 0.066 0.058 0.028 0.057 0.049 0.037 0.037 0.073
0.015 0.111 0.091 0.026 0.131 0.125 0.029 0.05 0.068
0.078 0.1 0.11 0.07 0.086 0.1 0.035 0.073 0.045
0.315 0.557 0.053 0.434 0.549 0.095 0.385 0.331 0.336
0.036 0.007 0.192 0.055 0.006 0.049 0.049 0.048 0.182
0.034 0.015 0.155 0.089 0.023 0.2 0.03 0.032 0.05
0.042 0.024 0.055 0.102 0.021 0.061 0.172 0.031 0.046
0.101 0.034 0.068 0.099 0.033 0.069 0.185 0.037 0.118
0.255 0.041 0.053 0.082 0.034 0.109 0.063 0.051 0.019
0.038 0.02 0.066 0.03 0.012 0.057 0.052 0.038 0.046
0.044 0.042 0.087 0.075 0.043 0.099 0.065 0.025 0.037
0.023 0.053 0.098 0.029 0.014 0.122 0.039 0.076 0.068
0.045 0.06 0.086 0.05 0.08 0.108 0.049 0.071 0.045
0.044 0.02 0.086 0.038 0.019 0.085 0.053 0.071 0.067
0.337 0.683 0.054 0.352 0.716 0.04 0.333 0.519 0.322
Spar-L-Settling
Spar-L-Org-production
Spar-L-Trapping
Spar-NonL-Settling
Spar-NonL-Org-production
Spar-NonL-Trapping
Mix-L-Settling
Mix-L-Org-production
Mix-L-Trapping
Fluxes in different scenarios
Fluxes in different scenarios
High
Parametric sensitivity
Low

Figure 8.

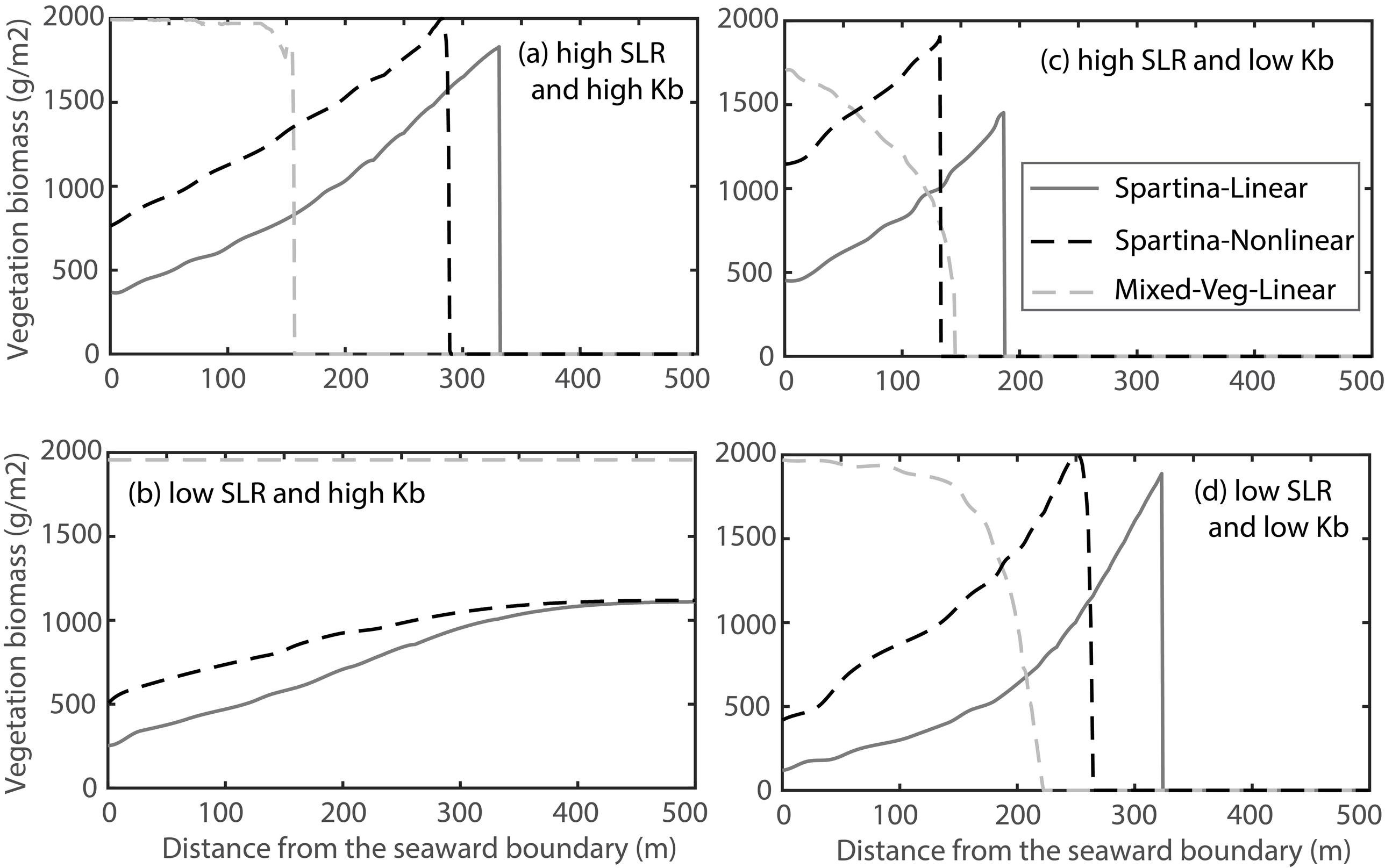
(a) high SLR and high Kb
(b) low SLR and high Kb
(c) high SLR and low Kb
(d) low SLR and low Kb
Spartina-Linear
Spartina-Nonlinear
Mixed-Veg-Linear
Vegetation biomass (g/m2)
Distance from the seaward boundary (m)
0
500
1000
1500
2000
0
100
200
300
400
500

Figure 9.

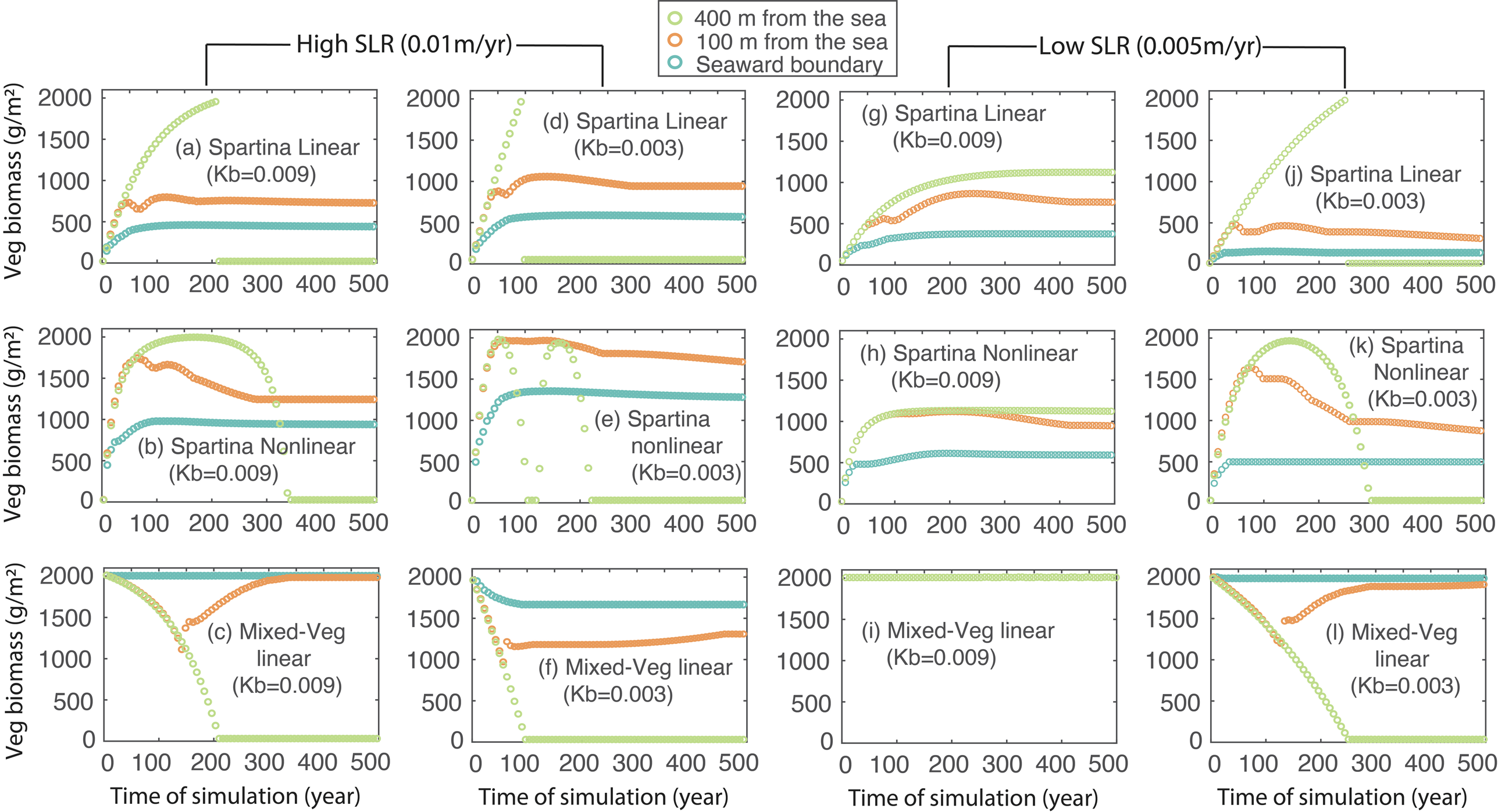
400 m from the sea
100 m from the sea
Seaward boundary
High SLR (0.01m/yr)
Low SLR (0.005m/yr)
Veg biomass (g/m²)
Time of simulation (year)
(a) Spartina Linear (Kb=0.009)
(b) Spartina Nonlinear (Kb=0.009)
(c) Mixed-Veg linear (Kb=0.009)
(d) Spartina Linear (Kb=0.003)
(e) Spartina nonlinear (Kb=0.003)
(f) Mixed-Veg linear (Kb=0.003)
(g) Spartina Linear (Kb=0.009)
(h) Spartina Nonlinear (Kb=0.009)
(i) Mixed-Veg linear (Kb=0.009)
(j) Spartina Linear (Kb=0.003)
(k) Spartina Nonlinear (Kb=0.003)
(l) Mixed-Veg linear (Kb=0.003)

Figure 10.

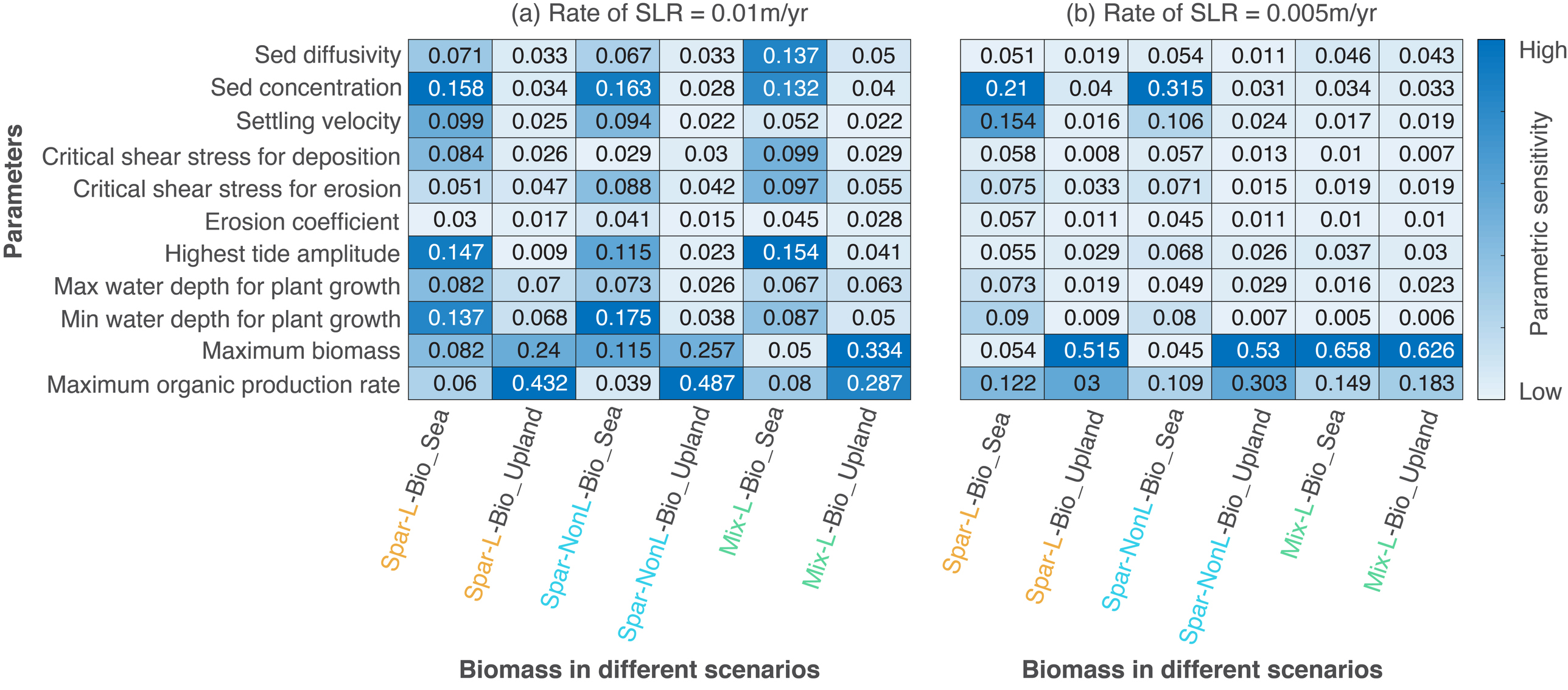
(a) Rate of SLR = 0.01m/yr
(b) Rate of SLR = 0.005m/yr
Parameters
Sed diffusivity
Sed concentration
Settling velocity
Critical shear stress for deposition
Critical shear stress for erosion
Erosion coefficient
Highest tide amplitude
Max water depth for plant growth
Min water depth for plant growth
Maximum biomass
Maximum organic production rate
0.071 0.033 0.067 0.033 0.137 0.05
0.158 0.034 0.163 0.028 0.132 0.04
0.099 0.025 0.094 0.022 0.052 0.022
0.084 0.026 0.029 0.03 0.099 0.029
0.051 0.047 0.088 0.042 0.097 0.055
0.03 0.017 0.041 0.015 0.045 0.028
0.147 0.009 0.115 0.023 0.154 0.041
0.082 0.07 0.073 0.026 0.067 0.063
0.137 0.068 0.175 0.038 0.087 0.05
0.082 0.24 0.115 0.257 0.05 0.334
0.06 0.432 0.039 0.487 0.08 0.287
0.051 0.019 0.054 0.011 0.046 0.043
0.21 0.04 0.315 0.031 0.034 0.033
0.154 0.016 0.106 0.024 0.017 0.019
0.058 0.008 0.057 0.013 0.01 0.007
0.075 0.033 0.071 0.015 0.019 0.019
0.057 0.011 0.045 0.011 0.01 0.01
0.055 0.029 0.068 0.026 0.037 0.03
0.073 0.019 0.049 0.029 0.016 0.023
0.09 0.009 0.08 0.007 0.005 0.006
0.054 0.515 0.045 0.53 0.658 0.626
0.122 03 0.109 0.303 0.149 0.183
Spar-L-Bio_Sea
Spar-L-Bio_Upland
Spar-NonL-Bio_Sea
Spar-NonL-Bio_Upland
Mix-L-Bio_Sea
Mix-L-Bio_Upland
Biomass in different scenarios
Biomass in different scenarios
High
Parametric sensitivity
Low